Meteoritics & Planetary Science 41, Nr 2, 263–284 (2006)
Abstract available online at http://meteoritics.org

Petrography and geochemistry of five new Apollo 16 mare basalts and evidence for post-basin deposition of basaltic material at the site

Ryan A. ZEIGLER[1*], Randy L. KOROTEV[1], Larry A. HASKIN[1], Bradley L. JOLLIFF[1], and Jeffrey J. GILLIS[2]

[1]Department of Earth and Planetary Sciences, Washington University in Saint Louis, Saint Louis, Missouri 63130–4862, USA
[2]Hawai'i Institute of Geophysics and Planetology, University of Hawai'i, Honolulu, Hawai'i 96822, USA
[*]Corresponding author. E-mail: zeigler@levee.wustl.edu

(Received 02 March 2005; revision accepted 24 August 2005)

Abstract–We present the petrography and geochemistry of five 2–4 mm basalt fragments from the Apollo 16 regolith. These fragments are 1) a high-Ti vitrophyric basalt compositionally similar to Apollo 17 high-Ti mare basalts, 2) a very high-Ti vitrophyric basalt compositionally similar to Apollos 12 and 14 red-black pyroclastic glass, 3) a coarsely crystalline high-Al basalt compositionally similar to group 5 Apollo 14 high-Al mare basalts, 4) a very low-Ti (VLT) crystalline basalt compositionally similar to Luna 24 VLT basalts, and 5) a VLT basaltic glass fragment compositionally similar to Apollo 17 VLT basalts. High-Ti basalt has been reported previously at the Apollo 16 site; the other basalt types have not been reported previously. As there are no known cryptomaria or pyroclastic deposits in the highlands near the Apollo 16 site (ruling out a local origin), and scant evidence for basaltic material in the Apollo 16 ancient regolith breccias or Apollo 16 soils collected near North Ray Crater (ruling out a basin ejecta origin), we infer that the basaltic material in the Apollo 16 regolith originated in maria near the Apollo 16 site and was transported laterally to the site by small- to medium-sized post-basin impacts. On the basis of TiO_2 concentrations derived from the Clementine UVVIS data, Mare Tranquillitatis (~300 km north) is the most likely source for the high-Ti basaltic material at the Apollo 16 site (craters Ross, Arago, Dionysius, Maskelyne, Moltke, Sosigenes, Schmidt), Mare Nectaris/Sinus Asperitatis (~220 km east) is the most likely source for the low-Ti and VLT basaltic material (craters Theophilus, Madler, Torricelli), and a large regional pyroclastic deposit near Mare Vaporum (~600 km northwest) is the most likely source region for pyroclastic material (although no source craters are apparent in the region).

INTRODUCTION

Of the nine locations on the Moon at which samples were collected by the Apollo and Luna missions, the Apollo 16 site in the feldspathic highlands is the most distant from an exposure of basalt (Fig. 1). The nearest mare shoreline to the Apollo 16 site is approximately 220 km to the northeast. A few fragments of basalt have been recovered in the Apollo 16 regolith samples (Delano 1975; Dowty et al. 1974a; Dowty et al. 1974b; Murali et al. 1976; Takeda et al. 1987; Galindo 1985; Simon and Papike 1987; Vaniman et al. 1978; Roedder and Weiblen 1974) and despite their rarity, the basaltic materials of the Apollo 16 site are more than just a novelty. Their abundance and the timing of their deposition can be used to further our understanding of the distribution of lunar materials by impact processes. The compositions of the basaltic fragments provide information about the composition of the maria surrounding the Apollo 16 site, some of which (e.g., Mare Nectaris) were not otherwise sampled.

In this paper, we present the petrography and geochemistry of five new basaltic fragments from the Apollo 16 site. We also present evidence, based primarily on the Apollo 16 ancient regolith breccias and soils collected near North Ray Crater, that all (or nearly all) of the basaltic material at the Apollo 16 site was deposited at the site as ejecta from small- to medium-sized post-basin impacts into the surrounding maria. Finally, using remotely sensed TiO_2 and FeO concentrations derived from Clementine UVVIS data, we identify likely provenances for the various types of basaltic material in the Apollo 16 soils.

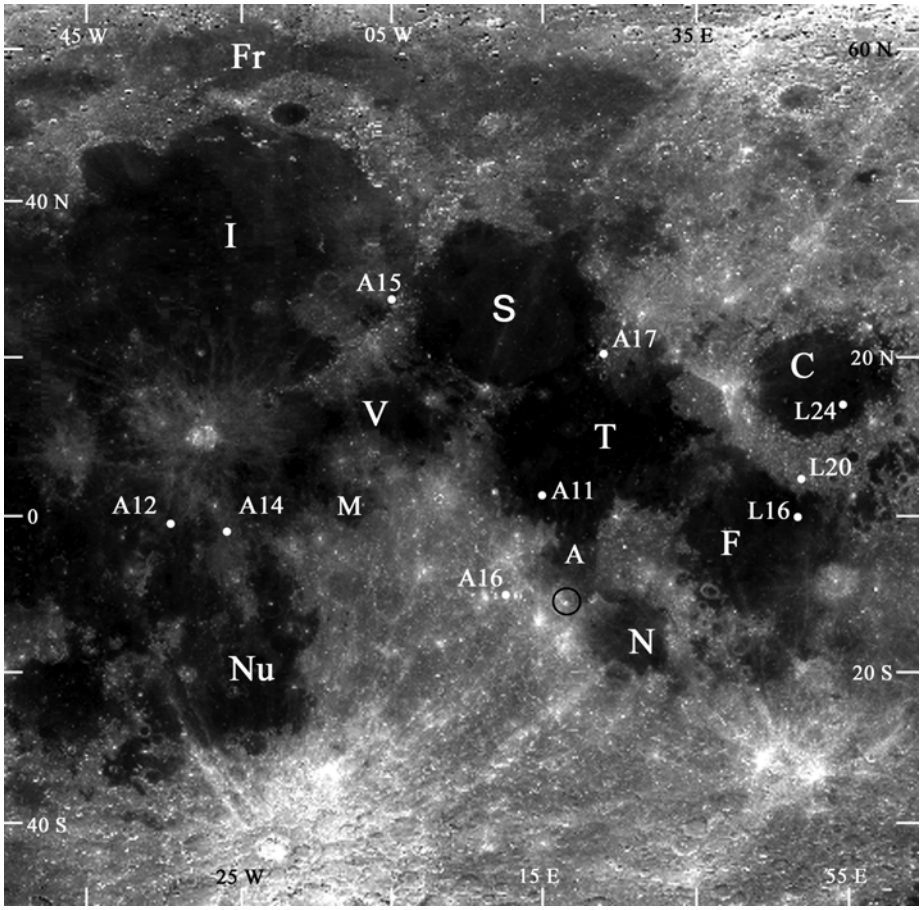

Fig. 1. A Clementine 750 nm image showing much of the lunar nearside. The sample return sites are labeled (A11 = Apollo 11; L16 = Luna 16; etc.), as well as some of the major mare filled basins (I = Imbrium, S = Serenitatis, N = Nectaris, T = Tranquillitatis, F = Fecunditatis, C = Crisium, Nu = Nubium, V = Vaporum, Fr = Frigoris, M = Sinus Medii, and A = Sinus Asperitatis). The black circle approximates the rim of the 100 km crater Theophilus.

SAMPLE SELECTION

The five basalt fragments described here are from a suite of 506 lithic fragments that we are studying from the 2–4 mm grain size fraction (sample numbers 6xxx3) of the Apollo 16 regolith. These samples originate from all of the sampling stations of the Apollo 16 site except stations 11 and 13 near North Ray Crater and from 21 of the 31 regolith samples collected at the surface or from trenches excavated at those stations. For all of the 21 regolith samples, the corresponding <1 mm fines (6xxx1) are either mature (15 samples) or submature (6 samples) with respect to surface exposure (Morris 1978).

The suite of fragments described here is not intended to be a representative subsample of the 2–4 mm grain-size fraction. We hand-picked each fragment from sample splits containing many fragments. The selection of particles was deliberately biased against highly feldspathic anorthosites, plagioclase single crystals, glassy fragments (including agglutinates and spherules), and fragments that were obviously multilithologic (dimict breccias, fragments with glass splash coatings). Although the fragment suite is not a lithologically representative sample of the 2–4 mm grain-size fraction of Apollo 16 soils, we suspect that, compositionally, it is also not highly biased in that the mean composition of all 506 lithic fragments is similar to the mean composition of mature <1 mm fines from Apollo 16 (Fig. 2).

ANALYTICAL METHODS

We analyzed the 506 lithic fragments for concentrations of 26 elements by instrumental neutron activation analysis (INAA) as we have done in similar studies in the past (Jolliff et al. 1991, 1996; Jolliff and Haskin 1995). We prepared each particle for analysis by ultrasonic rinsing in a bath of acetone to remove any dust coating, examination under a binocular microscope to make a preliminary lithologic classification, weighing, and sealing in a high-purity silica tube for neutron irradiation. The samples were irradiated at the University of Missouri—Columbia research reactor for 24–48 hr at a neutron flux of 5.15×10^{13} $cm^{-2}s^{-1}$. The methods for INAA are described more fully in Korotev (1991) and the methods

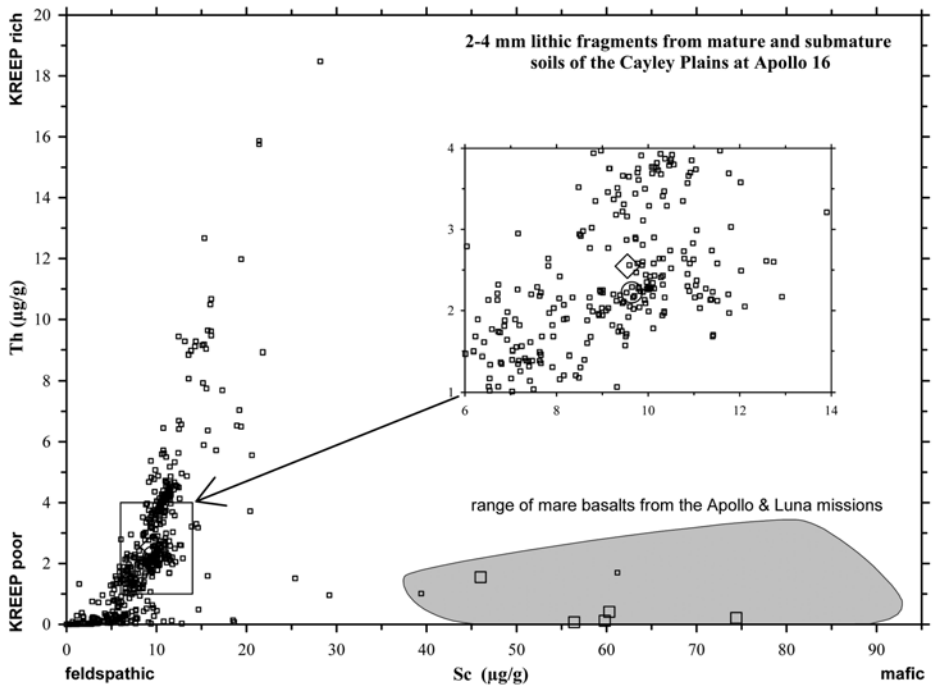

Fig. 2. Th and Sc concentrations in 506 2–4 mm lithic fragments from mature and submature regolith samples of the Cayley Plains at Apollo 16 site (squares; mean mass = 21 mg). The five large squares at high Sc concentration represent the mare lithologies described in the text. Other high-Sc points (small squares within the grey shaded area) represent mafic, nonmare lithologies (Zeigler et al. 2000). The range of Sc and Th concentrations in mare basalt from the Apollo and Luna mission is indicated by the gray field. The large circle represents the average composition of mature Apollo 16 soils (Korotev 1997) and the large diamond represents the mean composition of the 506 lithic fragments (best seen in inset). Fragments with Th concentrations exceeding ~3 ppm are mafic impact-melt breccias (Korotev 1994). Low-Sc, low-Th fragments are anorthosites, troctolites, and Fe,Ni metal fragments. Fragments with soil-like compositions (e.g., all points in the inset) are regolith breccias, fragmental breccias, granulitic breccias, and impact-melt breccias.

for data reduction are described in Lindstrom and Korotev (1982). Results of INAA are listed in Table 1.

After irradiation and radioassay, we prepared polished thin sections or grain mounts of five fragments that we suspected to be mare basalts on the basis of their compositions (e.g., high concentrations of Sc, Cr, and Fe) (Fig. 2). The fragments were characterized using the petrographic microscope in both transmitted and reflected light and electron microprobe analysis (EMPA) using a JEOL 733 electron microprobe. Characterization included backscattered electron (BSE) image analysis, energy-dispersive X-ray spectrum analysis, and quantitative mineral compositional analysis (feldspar, pyroxene, olivine, oxide, and glass) by wavelength-dispersive X-ray spectrometry (WDS). Mineral compositions were obtained at 15 kV accelerating voltage, 20, 30, or 40 nA beam current depending on the mineralogy of the target, and 1–20 µm electron beam spot size. A combination of mineral and oxide standards was used for calibration in WDS mineral analyses. Mineral compositional data obtained by WDS are included in Tables 2–6.

We prepared a fused bead to determine the major-element composition of some particles when a sufficient quantity of material (>5 mg) remained after thin-sectioning. We ground the remaining material of each fragment using an alumina mortar and pestle, fused the powder with a molybdenum strip resistance heater in an argon atmosphere, and mounted the resulting glass bead in epoxy. We then polished the fused beads and analyzed them with the electron microprobe using 15 kV accelerating voltage, 20 nA beam current, and 30–50 µm spot size to obtain major-element concentrations (for a more complete description, see Jolliff et al. 1996). Major-element concentrations of Apollo 16 mare basalts are listed in Table 1.

RESULTS

Petrography and Geochemistry of the New Apollo 16 Basalts and Comparison to Other Lunar Mare Basalts

The five basalt fragments of this study each differ from one another in composition and mineralogy. We describe them below.

Fragment 1: 60503,22-7

Fragment 60503,22-7 is a vitrophyric basalt containing xenocrysts of olivine (Fig. 3a). Modally, it consists of about 4% olivine grains in a groundmass of glass, ilmenite laths,

Table 1. Major-element and trace-element compositions of Apollo 16 basalts.

	60503,22–7	60603,10–16	62243,10–22	65703,9–13	60053,2–9
Traces by:	INAA	INAA	INAA	INAA	INAA
Majors by:	BB	FB	FB		MMR
Major element concentrations					
SiO_2	41.8	34.8	46.4		47.1
TiO_2	8.7	14.5	0.8	0.5	2.0
Al_2O_3	9.9	5.5	11.9		15.4
Cr_2O_3	0.49	0.83	0.55		0.06
FeO	18.4	23.0	18.6		18.0
FeO (INAA)	18.59	23.2	18.66	21.40	17.92
MnO	0.27	0.24	0.29		0.27
MgO	10.5	13.0	10.1		3.4
CaO	10.1	6.9	10.8		13.4
CaO (INAA)	10.7	7.2	11.8	12.1	14.3
Na_2O	0.30	0.46	0.20		0.35
Na_2O (INAA)	0.296	0.429	0.188	0.218	0.342
K_2O	0.02	0.17	<0.02		0.03
P_2O_5	n.a.	0.07	0.04		n.a.
Total	100.4	99.6	99.7		100.0
Trace element concentrations					
Sc	74.4	46	59.8	56.4	60.3
Cr	3750	6160	3830	2150	900
Co	43.4	57.4	30.1	21.6	20.8
Ni	130	<130	110	<190	<190
Sr	130	240	<200	<200	<240.
Zr	150	380	<160	<250	<500.
Ba	<90.	222	<50	<30	97
La	3.85	14.46	1.97	1.19	4.7
Ce	11.9	39.6	5.6	3.9	13
Nd	<24	35	<14	<30	9
Sm	5.47	11.35	1.338	1.098	3.54
Eu	1.14	2.56	0.39	0.47	1.02
Tb	1.55	2.38	0.34	0.32	0.91
Yb	5.93	5.79	1.84	1.9	5.17
Lu	0.9	0.775	0.282	0.282	0.763
Hf	5.14	11.05	0.96	0.84	2.79
Ta	0.94	2.61	0.11	<0.3	0.25
Ir	<15	<6	<10	<4	<5
Au	<12	<7	<8	<3	<3
Th	0.21	1.55	0.12	0.07	0.41
U	<0.7	0.45	<0.5	<0.17	0.21
Mass (mg)	56.79	33.94	15.29	20.37	23.81

FB: fused bead, BB: broad-beam EMPA, MR: modal recombination, MMR: modified modal recombination. Modified modal recombination involves using the observed mineral compositions to match the concentrations of major elements observed in the INAA chemistry (FeO, CaO, Na_2O, Cr_2O_3), yielding the concentrations of all of the major elements. Major element totals are based on EMPA data only. Broad-beam EMPA is the average composition of ~100 spots at 50 μm in the matrix. Oxides are given in wt%, Ir and Au in ng/g, and all others in μg/g. Average analytical uncertainties (representing 1 sigma estimates) for INAA data are: 1–3% for Na_2O, Sc, Cr, FeO, Co, La, Sm, Yb, and Lu; 3–6% for CaO, Ce, Eu, Tb, and Hf; 10% for BaO; 20–25% for Ta, Th, Nd, and Zr; 25–30% for Sr and U; and 40% for Ni. Less than values (<) represent twice the analytical uncertainty. n.a. = not analyzed.

and olivine with minor amounts of Cr-spinel and trace amounts of low-Ca pyroxene and Fe,Ni metal. The olivine grains occur in two distinct forms (Figs. 4a and 4b): larger, more magnesian grains (up to 0.4 mm in length, Fo_{72}) (Table 2) and somewhat smaller, more ferroan grains (~0.1 mm, $Fo_{62–57}$). Each large olivine grain is partially resorbed, is rimmed by olivine that zones outward from Fo_{77} to Fo_{68}, and is surrounded by a high concentration of thin ilmenite laths that radiate outward from the edges of the grains, which presumably served as nucleation sites (Figs. 4a and 4b). The groundmass consists of moderately TiO_2-rich glass (TiO_2 = 5.7 wt%) (Table 3) with abundant 1–2 μm wide ilmenite laths, elongated olivine grains <3 μm wide (Fo_{68}), and trace amounts of Cr-rich spinel (Fig. 4c; Table 4). Also

observed in the matrix are olivine grains that range in size up to 20 μm wide and 200 μm long. These grains are compositionally identical to the tiny matrix olivines and form intergrowths with ilmenite laths. A single pyroxene grain ($Wo_7En_{73}Fs_{20}$) (Table 5) occurs in the matrix. It has a irregular contact with the surrounding matrix and is likely being resorbed. The metal grains are tiny (a few μm), have ~9 wt% Ni, and a Ni/Co ratio of 10.6.

On the basis of experiments on the distribution of Fe and Mg between olivine and basaltic melts, the first olivine to crystallize from a melt with a bulk composition of 60503,22-7 (at low pressure) would have a composition of ~Fo_{79} (Longhi 1977; calculated using the Magpox program). When ilmenite comes on the liquidus the olivine composition would be ~Fo_{69}. The calculated initial olivine composition is close to the composition of the innermost rims on the large olivine grains (Fo_{77}) and the predicted olivine composition when ilmenite begins crystallizing is close to the outermost rim composition (Fo_{66}). This similarity in calculated and observed olivine compositions suggests that the rims on the large olivine grains were in equilibrium (or were reasonably close to equilibrium) with the melt from which they crystallized. The core compositions of the large olivine grains ($Fo_{60–72}$) are too ferroan to have crystallized early (as would be required given their large size relative to other minerals in the fragment) from a parent melt with the composition of 60503,22-7, indicating that they are xenocrysts rather than phenocrysts. A partially resorbed pigeonite grain is further evidence of xenocrysts in the fragment because only orthopyroxene was stable when the fragment quenched.

We estimated the bulk major-element composition of the fragment by averaging a large number (~100) of broad-beam spot (40–50 μm) analyses on traverses across the sample (Table 2). The major-element composition indicated by broad-beam analysis matches the major-element concentrations determined by INAA (FeO, CaO, Na_2O, and Cr_2O_3) well, providing confidence in the broad-beam estimate. On two-element discrimination plots (Figs. 5 and 6), sample 60503,22-7 lies within or near the field for the Apollo high-Ti basalts, and in most cases is more similar to Apollo 17 high-Ti basalts than to Apollo 11 high-Ti basalts. Relative abundances of rare earth elements (REE) are most similar to those of high-Ti basalts (Fig. 7a) and absolute abundances are more similar to those of Apollo 17 high-Ti basalts.

Fragment 60503,22-7 appears to be a rapidly crystallized high-Ti mare basalt that incorporated xenocrysts of olivine and pigeonite from older mare basalts. The rapid crystallization history is indicated by the glassy, fine-grained nature of the groundmass, which displays a variety of quench textures and glass compositions. There is no evidence of magma mixing. The high CaO concentrations of the olivine xenocrysts (~0.30 wt%) are consistent with a mare origin. At ~9 wt% Ni, the metal in 60503,22-7 is somewhat lower than typical of other olivine-rich basalts; however, the Ni/Co ratio of ~10 is similar (Papike et al. 1998). The lack of detectable Ir and Au in the whole particle (<15 ppb and <12 ppb, respectively) suggests that the fragment is not a partially quenched melt breccia produced by a meteoritic impact, although this possibility can not be ruled out.

Fragment 2: 60603,10-16

Fragment 60603,10-16 is a vitrophyric basalt (Fig. 3b) with phenocrysts of ilmenite, olivine, and minor Cr-rich spinel in a groundmass of glass, olivine, and trace Fe-metal (Fig. 4d). Subhedral olivine grains, up to ~60 μm across, have cores of Fo_{78} and rims of Fo_{63} (Table 2). Ilmenite crystals up to 200 μm long commonly display skeletal textures (Fig. 4d). Minor equant spinel (<25 μm) has ~22 wt% Cr_2O_3 and a Cr:Ti:Fe ratio of ~1:1:2 (Table 4). One edge of the fragment (Fig. 3b, right side) has greater porosity than the rest of the grain, a smaller grain size (particularly in ilmenite) (Fig. 4e), and slightly more ferroan olivine cores (Fo_{76} versus Fo_{78}). Throughout the fragment, the glass has a ferroan, moderately TiO_2-rich composition (Mg' = 31.7; TiO_2 = 6.6 wt%) (Table 3). Tiny (as small as 1–2 μm) anhedral olivine grains with compositions in the same range as the rims of the olivine phenocrysts are found throughout the fragment. The Fe-metal grains in the fragment are tiny (<2 μm) and have ~1 wt% Co and 1–6 wt% Ni.

The glassy groundmass, the skeletal texture of ilmenite grains, and the zoning in the olivine reflect rapid crystallization. The greater porosity and smaller grain size along one edge of the sample suggests that this edge cooled more rapidly than the rest of the fragment and likely represents the original edge of the fragment after crystallization. The slightly more ferroan nature of the olivine found along this edge is at odds with this interpretation (which should be more magnesian, since it crystallized first); however, the difference is small (Fo_{78} versus Fo_{76}) and may be a sampling error. The lack of a "chilled margin" on the other sides of the particle simply reflects that this is a small piece of a larger object.

Concentrations of FeO and TiO_2 (23.0 wt% and 14.5 wt%, respectively) are greater than those of any well-sampled basalt type, but are similar to those of some very high-Ti picritic glasses, particularly the red-black glasses of Apollos 12 and 14, albeit with a slightly lower TiO_2 concentration (Fig. 5a) (Marvin and Walker 1978; Delano 1986; Shearer and Papike 1993). Concentrations of heavy REEs are strongly depleted in a manner characteristic of high-Ti picritic glasses (Fig. 7b). Fragment 60603,10-16 has concentrations of Na, Ba, Sm, and Cr similar to those of Apollo 12 and 14 red-black glasses, but has a slightly lower Sc concentration (Fig. 6).

The rapidly crystallized nature of fragment 60603,10-16, the presence of an apparent chilled margin, the major- and trace-element compositions, and the mineral chemistry support an origin for the fragment as a product of a pyroclastic

Table 2. Olivine compositions and stoichiometry.

Sample	60503,22-7	60503,22-7	60503,22-7	60503,22-7	60503,22-7	60603,10-16	60603,10-16	60603,10-16	60603,10-16	65703,9-13	65703,9-13	65703,9-13	60053,2-9
Description	Fe-Xe	Fe-Xe	Mg-Xe	I-rim	O-rim	Cores	CZ	Rims	Matrix	Mg-end	Mid	Fay.	Fay.
N	(3)	(3)	(8)	(12)	(8)	(10)	(3)	(9)	(3)	(1)	(1)	(1)	(5)
Oxide concentrations													
SiO_2	36.35	37.02	38.37	38.75	37.28	38.90	38.72	37.20	36.44	34.35	36.82	30.04	30.23
TiO_2	0.14	0.11	0.07	0.23	0.59	0.42	0.47	0.50	0.49	0.05	0.02	0.24	0.33
Al_2O_3	0.02	<0.02	<0.02	0.03	0.17	0.05	0.04	<0.02	0.03	<0.02	0.03	<0.02	<0.02
Cr_2O_3	0.24	0.28	0.40	0.33	0.40	0.45	0.35	0.25	0.15	0.26	0.27	0.02	0.06
FeO	35.30	31.95	24.54	21.35	26.87	19.62	21.87	29.63	32.28	42.15	32.07	66.37	66.07
MnO	0.43	0.45	0.29	0.22	0.29	0.22	0.21	0.33	0.29	0.61	0.28	0.91	0.96
MgO	26.97	29.70	36.16	38.34	33.32	40.08	38.67	31.77	29.92	21.18	30.14	0.59	1.77
CaO	0.29	0.31	0.31	0.34	0.44	0.26	0.31	0.43	0.55	0.54	0.41	0.99	0.35
Na_2O	<0.02	<0.02	<0.02	<0.02	<0.02	<0.02	<0.02	<0.02	<0.02	<0.02	<0.02	<0.02	<0.02
Total	99.79	99.83	100.16	99.60	99.35	100.01	100.63	100.12	100.15	99.14	100.04	99.16	99.77
Mg′	57.7	62.4	72.4	76.2	68.9	78.5	75.9	65.7	62.3	47.3	62.6	1.5	4.6
Cations per 4 oxygen atoms													
Si	1.012	1.012	1.016	1.007	1.000	0.999	0.999	1.003	0.996	1.003	1.005	1.013	1.007
Al	0.001	<0.001	<0.001	0.001	0.005	0.002	0.001	<0.001	0.001	<0.001	0.001	<0.001	<0.001
Ti	0.003	0.002	0.001	0.005	0.012	0.008	0.009	0.010	0.010	0.001	<0.001	0.006	0.008
Cr	0.005	0.006	0.006	0.007	0.008	0.009	0.007	0.005	0.003	0.006	0.006	0.001	0.001
Fe^{2+}	0.822	0.731	0.533	0.464	0.603	0.422	0.472	0.670	0.738	1.029	0.733	1.871	1.840
Mn^{2+}	0.010	0.010	0.006	0.005	0.007	0.005	0.005	0.007	0.007	0.015	0.006	0.026	0.027
Mg	1.119	1.211	1.411	1.486	1.332	1.535	1.487	1.275	1.220	0.922	1.227	0.029	0.088
Ca	0.009	0.009	0.008	0.010	0.013	0.007	0.009	0.013	0.016	0.017	0.012	0.036	0.013
Na	<0.001	<0.001	<0.001	<0.001	<0.001	<0.001	<0.001	<0.001	<0.001	<0.001	<0.001	<0.001	<0.001
Oct Sum	1.969	1.970	1.965	1.977	1.981	1.988	1.989	1.981	1.995	1.990	1.985	1.968	1.978
Sum all	2.982	2.982	2.980	2.984	2.981	2.987	2.988	2.984	2.998	2.993	2.991	2.981	2.984
Endmember proportions													
Fa	42.3	40.0	35.5	33.7	35.7	21.6	24.1	34.5	37.7	52.7	37.4	98.5	95.4
Fo	57.7	60.0	64.5	66.3	64.3	78.4	75.9	65.5	62.3	47.3	62.6	1.5	4.6

The two Fe-rich olivine xenocrysts (Fe-Xe) in sample 60503,22-7 have different compositions. All Mg-rich olivine xenocrysts (Mg-Xe) have the same composition. Also in 60503,22-7, the composition of the magnesian (inner) and ferroan (outer) rims on the xenocrysts are given (I-rim, O-rim). The olivine found in the matrix of 60503,22-7 is compositionally indistinguishable to the Fe-rims, and the values are averaged. In 60603,10-16, the cores of most of the olivine grains in the sample (Cores) and the cores in the chilled zone (CZ) have slightly different compositions. The more ferroan rims on all of these olivine grains (Rims) and the small anhedral matrix olivine grains (Matrix) are also presented here. The olivine in 65703,9-13 is strongly zoned, so averages could not be presented. Instead, the two end-member compositions (Mg-end, Fay.) and one intermediate composition (Inter.) are listed. Finally, the fayalite (Fay.) in 60053,2-9 is shown. N is the number of analyses averaged into the listed composition. Mg′ = molar Mg/(Fe + Mg)*100.

Table 3. Glass compositions.

	60503,22-7	60603,10-16	62243,10-22	62243,10-22	60053,2-9	60053,2-9
Description	Dark	Glass	Mottled	Plain	P vein	Q vein
N	(6)	(11)	(12)	(11)	(7)	(2)
SiO_2	45.38	48.18	46.33	46.49	45.38	42.54
TiO_2	5.70	6.62	0.83	0.83	0.79	1.71
Al_2O_3	10.83	9.58	11.88	11.83	15.53	3.87
Cr_2O_3	0.28	0.12	0.56	0.53	0.19	0.10
FeO	14.96	15.71	18.64	18.64	20.22	37.81
MnO	0.23	0.24	0.30	0.28	0.29	0.49
MgO	8.72	4.10	10.17	9.94	4.30	3.19
CaO	13.14	14.07	10.80	10.83	12.63	9.22
Na_2O	0.28	0.77	0.20	0.19	0.38	0.14
K_2O	<0.02	0.26	<0.02	<0.02	<0.02	<0.02
Total	99.52	99.65	99.71	99.57	99.71	99.07

The dark glass listed for sample 60503,22-7 is the "typical" dark glass found interstitial to the ilmenite laths in the groundmass. The "mottled" and "plain" glass compositions listed for basalt vitrophyre 62243,10-22 are representative of the two morphologies of this sample. They are virtually identical in composition. The glass veins found in the plagioclase (P vein) and quartz (Q vein) of sample 60053,2-9 have different compositions.

Table 4. Oxide concentrations and stoichiometry.

Sample	60503,22-7	60603,10-16	60603,10-6	65703,9-13	65703,9-13	60053,2-9
Description	Cr spinel	Cr spinel	Mg ilmenite	Cr spinel	Ulvöspinel	Ilmenite
N	(3)	(4)	(3)	(2)	(2)	(4)
Oxide concentrations						
FeO	32.25	40.17	37.54	30.59	65.68	46.38
MgO	9.17	6.75	5.58	5.22	<0.02	0.22
Cr_2O_3	29.47	23.48	1.70	39.22	<0.02	<0.02
TiO_2	16.11	24.31	54.38	2.75	31.08	52.64
MnO	0.29	0.34	0.41	0.32	0.44	0.51
V_2O_3	0.49	0.23	<0.02	0.84	<0.02	<0.02
Al_2O_3	10.77	4.83	0.21	19.83	1.81	0.07
CaO	0.38	0.18	0.34	0.32	0.38	0.05
ZnO	<0.02	<0.02	<0.02	<0.02	<0.02	<0.02
SiO_2	0.51	0.13	0.11	0.20	0.26	0.05
Total	99.43	100.41	100.27	99.28	99.67	99.93
Cations per 4 oxygen atoms (spinel) or 3 oxygen atoms (ilmenite)						
Si IV	0.017	0.004	0.003	0.007	0.010	0.001
Al VI	0.419	0.194	0.006	0.772	0.080	0.002
Ti	0.400	0.622	0.983	0.068	0.880	0.998
V	0.013	0.006	0.000	0.022	0.000	0.000
Cr	0.769	0.631	0.032	1.024	0.000	0.000
Fe^{2+}	0.891	1.142	0.754	0.845	2.069	0.978
Mn^{2+}	0.008	0.010	0.008	0.009	0.014	0.011
Mg	0.452	0.342	0.200	0.257	0.000	0.008
Zn	0.000	0.000	0.000	0.000	0.000	0.000
Ca	0.013	0.007	0.009	0.011	0.015	0.001
Sum 2+	1.364	1.501	0.971	1.122	2.099	0.998
Sum 3,4+	1.619	1.458	1.024	1.894	0.971	1.002
Sum Oct.	2.965	2.954	1.993	3.009	3.060	1.998

eruption. The lack of detectable Ir and Au (<6 ppb and <7 ppb, respectively) in the fragment and the Ni/Co ratios of the metal grains argue against an origin as an impact melt formed by meteoritic impact into a basaltic target.

Fragment 3:62243,10-22

Fragment 62243,10-22 is a basaltic vitrophyre of VLT composition that is pervasively fractured to the point of being friable. The fragment disaggregated in the silica tube used for INAA during analysis. All seven subfragments in the grain mount we analyzed by EMPA appeared to be entirely glassy except for one area of what appears to be quenched pyroxene and trace amounts of Fe,Ni metal. The proposed pyroxene crystallized rapidly, as indicated by its "graphic" texture (with intersertal glass) (Fig. 4f) and high Al_2O_3 concentrations (~7 wt%). Due to rapid crystallization, the stoichiometry of

Table 5. Pyroxene compositions and stoichiometry.

Sample	60503,22-7	62243,10-22	65703,9-13	65703,9-13	65703,9-13	65703,9-13	60053,2-9	60053,2-9	60053,2-9	60053,2-9	60053,2-9	60053,2-9
Description	Xeno	Quench	Mg-rich	Fe-rich	Inter.	Inter.	Hd	Inter.	Inter.	Inter.	Inter.	Symp
N	(2)	(9)	(1)	(1)	(1)	(1)	(4)	(17)	(18)	(6)	(8)	(1)
Oxide concentrations												
SiO_2	54.87	42.37	49.29	45.51	48.11	46.63	48.11	50.54	48.63	46.97	47.35	50.75
TiO_2	0.86	0.64	1.08	1.28	1.56	1.16	0.92	0.53	0.90	0.96	1.05	0.32
Al_2O_3	0.75	7.34	4.09	1.95	3.74	2.43	0.72	1.28	1.05	1.00	1.04	0.25
Cr_2O_3	0.57	0.78	0.84	0.16	0.67	0.25	0.05	0.56	0.26	0.06	0.04	<0.02
FeO	12.84	26.42	15.09	39.43	20.35	33.12	29.70	25.41	30.89	34.76	32.21	40.67
MnO	0.24	0.36	0.31	0.64	0.39	0.48	0.48	0.45	0.52	0.49	0.44	0.60
MgO	26.93	15.87	10.45	0.05	7.70	3.35	2.24	13.26	7.00	2.85	1.60	1.55
CaO	2.87	6.29	18.39	11.11	17.33	12.25	17.82	7.88	10.56	12.46	15.78	6.53
Na_2O	<0.02	0.09	0.02	<0.02	<0.02	<0.02	0.04	0.02	0.02	0.02	0.02	<0.02
Total	99.94	100.15	99.56	100.15	99.84	99.67	100.09	99.93	99.83	99.58	99.51	100.67
Cations per 4 oxygen atoms												
Si	1.969	1.667	1.888	1.922	1.882	1.919	1.968	1.961	1.961	1.953	1.962	2.082
Al	0.031	0.198	0.135	0.091	0.142	0.099	0.031	0.053	0.049	0.047	0.049	0.012
Ti	0.000	0.000	0.000	0.000	0.000	0.000	0.000	0.000	0.000	0.000	0.000	0.000
Sum Tetra.	2.000	1.865	2.024	2.013	2.025	2.017	1.999	2.013	2.009	2.000	2.012	2.094
Al VI	0.001	0.142	0.049	0.006	0.030	0.019	0.003	0.006	0.001	0.002	0.001	0.000
Ti VI	0.023	0.019	0.031	0.041	0.046	0.036	0.028	0.016	0.027	0.030	0.033	0.010
Cr	0.016	0.025	0.025	0.005	0.021	0.008	0.002	0.017	0.008	0.002	0.001	0.000
Fe^{2+}	0.385	0.870	0.484	1.392	0.666	1.140	1.016	0.824	1.042	1.209	1.117	1.395
Mn^{2+}	0.007	0.012	0.010	0.023	0.013	0.017	0.017	0.015	0.018	0.017	0.015	0.021
Mg	1.441	0.932	0.597	0.003	0.449	0.205	0.137	0.767	0.420	0.177	0.099	0.095
Ca	0.110	0.265	0.755	0.502	0.727	0.540	0.781	0.328	0.456	0.555	0.701	0.287
Na	0.001	0.007	0.002	0.001	0.000	0.001	0.003	0.001	0.001	0.002	0.001	0.000
Sum M1,M2	1.969	2.271	1.953	1.974	1.951	1.966	1.974	1.973	1.967	1.986	1.960	1.804
Endmember proportions												
Wo	34.1	12.9	33.8	24.6	25.7	39.0	25.5	25.7	27.6	35.0	29.8	19.4
En	36.4	45.0	26.7	0.2	11.3	7.2	4.7	21.4	9.2	5.3	39.1	38.9
Fs	29.5	42.1	39.5	75.2	63.0	53.8	69.8	52.9	63.1	59.7	31.1	41.8

One partially resorbed pyroxene was found in 60503,22-7, likely representing a xenocryst (Xeno). The average composition of the quench crystallized very high-Al pyroxene in 62243,10-22 (Quench) has, not unexpectedly, poor stoichiometry. The pyroxene in 65703,9-13 is widely zoned, and analyses representing the magnesian and ferroan end-members (Mg-rich, Fe-rich) and several intermediate (Inter.) compositions are listed. The four compositions listed for sample 60053,2-9 represent arbitrary groupings of the data that fell in the same area of the quadrilateral. Also shown are the average composition of the hedenbergite in the symplectite (Hd) and the composition of the bulk symplectite region (symp).

Table 6. Feldspar compositions and stoichiometry.

Sample	65703,9-13	60053,2-9	60053,2-9	60053,2-9
Description	Average	Average	Near veins	Quartz
N	(7)	(5)	(1)	(1)
Oxide concentrations				
SiO_2	45.18	44.96	46.82	98.85
TiO_2	–	–	–	0.20
Al_2O_3	34.23	34.90	33.51	0.22
FeO	1.19	0.57	0.92	0.03
MgO	0.38	0.10	<0.02	0.03
CaO	18.39	18.86	17.59	<0.02
Na_2O	0.58	0.61	1.09	0.05
K_2O	<0.02	0.02	0.22	0.15
Total	100.0	100.2	100.3	99.53
Cations per 8 oxygen atoms				
Si	2.093	2.078	2.156	–
Al	1.869	1.901	1.819	–
Sum Tetra.	3.962	3.979	3.974	–
Fe^{2+}	0.046	0.022	0.035	–
Mg	0.026	0.007	0.000	–
Ca	0.913	0.934	0.868	–
Na	0.052	0.055	0.097	–
K	0.000	0.001	0.013	–
Sum Others	1.037	1.018	1.014	–
Endmember proportions				
An	94.6	94.4	88.7	–
Ab	5.4	5.5	9.9	–
Or	0.0	0.1	1.4	–

Typically, most of the plagioclase in 60053,2-9 and 65703,9-13 was not strongly zoned, and did not deviate from the listed averages by more than ±0.6 An. The plagioclase compositions near the glass veins that cut across plagioclase in 60053,2-9 showed an increase in Fe and Na, however. The composition of the crystalline silica phase (likely quartz) in 60053,2-9 is also listed here. Tetra = tetrahedral site.

the pyroxene is poor (Table 5). The glass in the fragment shows two morphologies: a dark-light mottled texture and a homogeneous texture. Broad-beam EMPA of the two morphologies show them to be compositionally indistinguishable when analyzed with a 40 μm diameter beam (Table 3). The metal grains are tiny (~1 μm) and contain ~3.2 wt% Ni with a Ni/Co ratio of 3.5. Because the nominal beam size is also ~1 μm, it overlaps slightly onto the surrounding silicates, and the Ni concentration should be viewed as a lower limit. The Ni/Co ratio would be unaffected, however, as the glass that surrounds the metal grains has insignificant Co and Ni concentrations compared to the metal grains.

The composition of fragment 62243,10-22 does not match that of any previously recognized pyroclastic (volcanic) glass. The Al_2O_3 concentration is high (11.9 wt%) and the MgO/A_2O_3 ratio (0.84) is low when compared to the maximum Al_2O_3 concentration and the MgO/Al_2O_3 ratios (10.3 wt% and 1.2–3.8, respectively) in the known pyroclastic glass groups (Delano 1986; Shearer and Papike 1993). However, the major-element (e.g., FeO, TiO_2, Na_2O) (Figs. 5a and 5b) and ferromagnesian trace-element compositions (e.g., Cr, Sc) (Fig. 6b) of 62243,10-22 are similar to VLT basalt fragments found at the Apollo 17 site (Wentworth et al. 1979; Jolliff et al. 1996). Furthermore, concentrations of incompatible trace elements (e.g., Sm, Ba) (Figs. 6a and 6c) are similar to those in VLT basalts and the relative abundances of REE are nearly identical to those of Apollo 17 VLT basalts (Fig. 7c).

Fragment 62243,10-22 appears to be a piece of a quenched basalt similar to the Apollo 17 VLT basalts. The lack of detectable Ir and Au in the fragment and the low Ni/Co ratio of the metal argue against an origin by meteoritic impact, unless little meteoritic material was incorporated into the resulting melt.

Fragment 4: 65703,9-13

Fragment 65703,9-13 is a highly fractured, slightly friable, crystalline basalt of VLT composition. It is composed of plagioclase, olivine, and pyroxene, with trace amounts of fayalite, Cr-rich spinel, troilite, and ilmenite. On the basis of BSE image analysis, the fragment has a mode of ~45% plagioclase and approximately equal amounts of olivine and pyroxene (these minerals exhibit wide, overlapping brightness ranges in BSE images, making an exact mode impossible to determine); all other phases make up <0.1% of the sample. The texture is subophitic (Fig. 3c) with elongated plagioclase grains of nearly uniform composition ($An_{94.6}$)

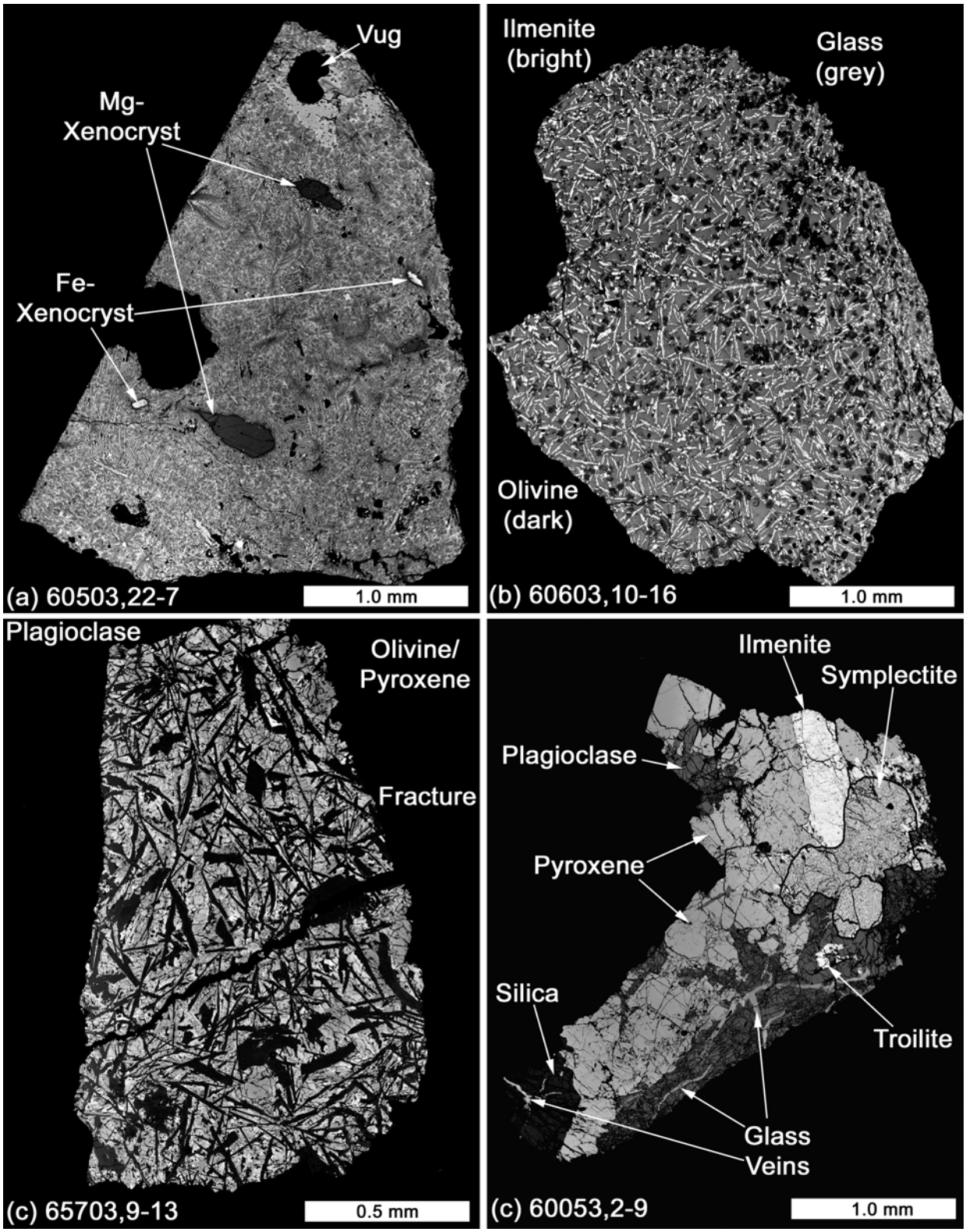

Fig. 3. Backscattered electron (BSE) images of 4 basalt samples in this study. a) High-Ti mare basalt vitrophyre 60503,22-7 with olivine xenocrysts in a matrix of ilmenite, glass, and olivine. b) Very high-Ti basaltic vitrophyre 60603,10-16 with skeletal ilmenite and subhedral olivine grains in a glassy matrix. Vesicular area along the right edge is likely a chilled margin. c) Crystalline VLT mare basalt with uniform plagioclase and widely zoned olivine and pyroxene grains. d) Shocked high-Al basalt 60053,2-9 with coarse-grained plagioclase and pyroxene, modal and normative silica, and fayalite-hedenbergite-silica symplectite (outlined in black).

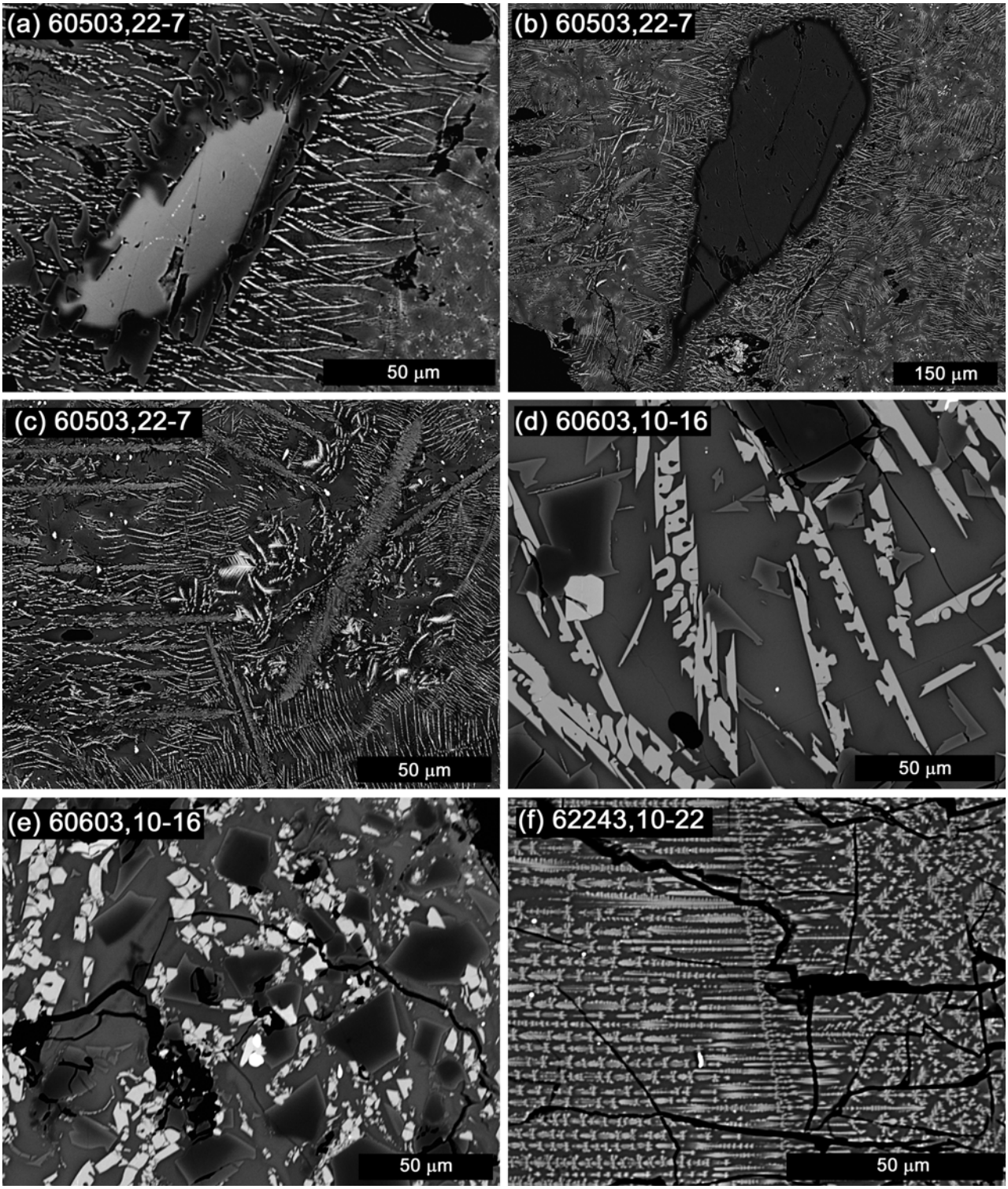

Fig. 4. BSE images of textures and chemical zoning in the basalts of this study. a) An Mg-rich olivine xenocryst that is partially resorbed in mare basalt vitrophyre 60503,22-7. b) More ferroan olivine xenocryst partially resorbed in 60503,22-7. c) A close-up of the quenched mesostasis of 60503,22-1; ilmentite laths are the brighter, thinner grains, whereas the quenched olivine grains are somewhat larger. d) Close-up of mesostasis in basaltic vitrophyre 60603,10-16 showing skeletal ilmenite grains (bright), equant Cr-spinel grains (bright), subhedral olivine phenocrysts (dark), and tiny anhedral olivine grains all in a glassy matrix. e) The mesostasis near the vesicular edge of 60603,10-16. This area has increased porosity and smaller olivine and ilmenite grains than the interior. f) Very high-Al “graphic” pyroxene (bright) set in VLT glass in basalt vitrophyre 62243,10-22.

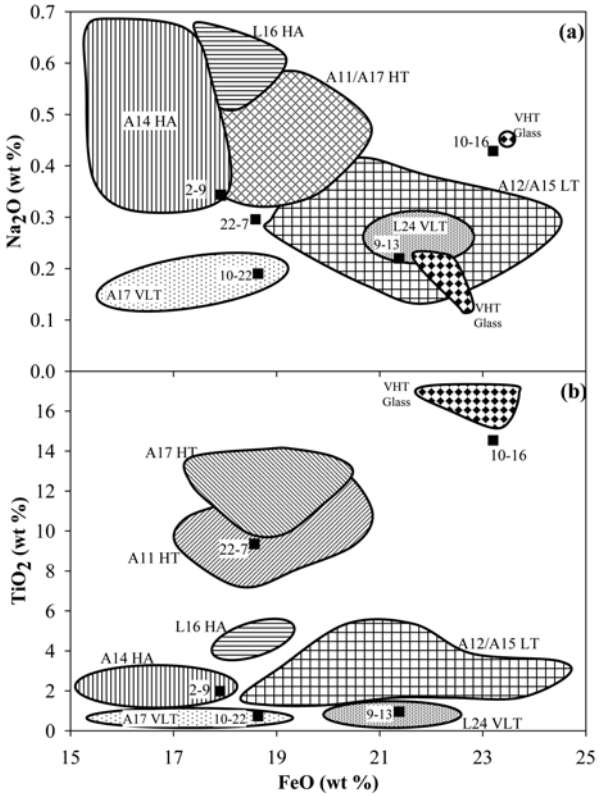

Fig. 5. Major-element discrimination plots showing the fields for the known mare basalt types with the samples from this study superimposed. Data in this and all subsequent figures from an unpublished compilation of Korotev. a) FeO versus Na_2O: 60053,2-9 falls within the field of Apollo 14 high-Al basalts, 65703,9-13 and 62243,10-22 fall in the fields for Luna 24 and Apollo 17 VLT basalts respectively, 60603,10-16 is similar to the composition of one of the Apollo 14 red-black glass groups, and 60503,22-7 falls just below the field for high-Ti mare basalts. b) FeO versus TiO_2: 65703,9-13 and 62243,10-22 again fall within the fields of Luna 24 and Apollo 17 VLT basalts respectively, 60503,22-7 falls in the high-Ti basalt field, 60603,10-16 falls close to the Apollo 12 and 14 pyroclastic glasses, albeit with slightly lower TiO_2, concentrations, and 60053,2-9 falls within the Apollo 14 high-Al basalt field.

(Table 6) partially enclosed by strongly zoned olivine ($Fo_{7–62}$) (Table 2) and pyroxene ($Wo_{31}En_{38}Fs_{31}$-$Wo_{22}En_1Fs_{77}$) (Table 5; Fig. 8). Pyroxene grains typically surround olivine in an apparent reaction texture. The wide range in olivine compositions is similar to Luna 24 VLT ferrobasalts, whereas the pyroxene crystallization trends are similar to the Apollo 17 VLT basalts (Papike and Vaniman 1978). Fayalite and several oxide grains (in order of decreasing abundance: Cr-rich spinel, troilite, and ulvöspinel) are present as 1–2 μm interstitial grains.

Modal recombination yields a bulk TiO_2 concentration for the fragment of ~0.5 wt%, as calculated from the average TiO_2 concentrations observed in the silicates (~0.1 wt% in olivine, ~1.3 wt% in pyroxene, ~0 wt% in plagioclase), the mode of the fragment (assuming an equal amount of olivine and pyroxene), and the paucity of ilmenite. The strongly zoned nature of the mafic silicates and relatively coarse grain size precludes an accurate estimation of other major element concentrations by modal recombination or broad beam EMPA. Those major-element concentrations that we determine by INAA (e.g., FeO, TiO_2, Na_2O) (Fig. 5) show fragment 65703,9-13 to be compositionally similar to the VLT basalts from Luna 24 (Ma et al. 1978; Blanchard et al. 1978). Ferromagnesian trace-element concentrations (Fig. 6b) in 65703,9-13 are also consistent with those of Luna 24 VLT basalts. Concentrations of ITEs are similar to those of VLT basalts (Figs. 6a and 6c) and REE abundances of 65703,9-13 are more similar to those of Luna 24 VLT basalts than Apollo 17 VLT basalts, particularly as they both have positive Eu anomalies. However, fragment 65703,9-13 is relatively enriched in heavy REE compared to the Luna 24 basalts.

On the basis of the geochemistry and observed mineralogy, 65703,9-13 is a VLT basalt that is similar to the Luna 24 VLT basalts. Geochemically, the positive Eu anomaly, very low-Ti concentrations, and Fe-rich nature are the most striking similarities to Luna 24 VLT basalts. Petrologically, subophitic textures like that in fragment 65703,9-13 are common in Luna 24 mare basalts, as are strongly zoned olivine ($Fo_{58–5}$) (Papike and Vaniman 1978).

Fragment 5: 60053,2-9

Fragment 60053,2-9 is a coarse-grained basalt (Fig. 3d). Modally, the fragment has about 50% pyroxene, 25% plagioclase 13% groundmass, 6% silica, and 6% ilmenite. Traces of troilite and glass veins (likely produced by localized shock melting) are also present. The pyroxene is coarse (up to 1 mm) and compositions range from calcic pigeonite ($Wo_{18.5}En_{42}Fs_{49.5}$) to ferroaugite ($Wo_{36.5}En_{4.5}Fs_{59}$) (Fig. 8b). The most magnesian pyroxenes have submicron exsolution lamellae. The pyroxene zoning trend in 60053,2-9 is similar to that observed in the Apollo 14 high-Al basalts (Papike and Vaniman 1978). The plagioclase is strongly fractured, although originally coarse-grained (up to 1 mm), with veins of shock-melted glass (Table 3) running through it. The plagioclase has a uniform composition ($An_{94}Or_{<0.2}$) (Table 6) except near the glass veins, where it is more alkalic ($An_{88}Or_1$). A single, large, crystalline SiO_2 grain is present. It is strongly fractured and has an Fe-rich vein of glass running through it. The silica phase contains <0.2 wt% each of K_2O, TiO_2, and Al_2O_3 (Table 6). We tentatively identify the silica grain as quartz on the basis of its optical properties (uniaxial negative). Ilmenite occurs mainly as a single, large, elongated grain (~600 μm long), but a few smaller (<30 μm) grains are also present. One ~50 μm grain of troilite is present in the thin section. The groundmass is a symplectic intergrowth of fayalite (Fo_5), hedenbergite ($Wo_{40}En_7Fs_{53}$), and silica. We interpret the symplectite to be a breakdown product from slow cooling of pyroxferroite (Table 5) (Jolliff et al. 1998).

The major-element composition is estimated using a modified modal recombination approach where the observed mineral compositions in 60053,2-9 are combined in proportions that reproduce the concentrations of major elements determined by INAA (FeO, CaO, Na_2O, and Cr_2O_3). With 15 wt% Al_2O_3, fragment 60053,2-9 is a high-Al basalt by lunar standards. Given the small size and coarse-grained nature of this sample, the bulk major-element concentrations may not be representative of the parent basalt, however, which may account for the unusually low MgO concentrations in this sample (3.4 wt%). Nevertheless, concentrations of FeO, TiO_2, and Na_2O (Fig. 5) are similar to those of Apollo 14 high-Al basalts (Dickinson et al. 1985; Shervais et al. 1985). Most trace-element concentrations are similar to those of the group 5, Apollo 14 high-Al basalts (Fig. 6). An exception is that of Cr (900 ppm), which is low compared to any type of mare basalt. The REE pattern of 60053,2-9 is most similar to that of the group 5 high-Al basalts of Apollo 14; absolute concentrations are slightly greater, however (Fig. 7e).

Fragment 60053,2-9 is most similar to Apollo 14–like high-Al basalts, especially the compositional group 5 of Dickinson et al. (1985). In addition to the geochemical similarities, the mineral assemblage in 60053,2-9, the texture, and the mineral compositions fall within the range previously observed in Apollo 14 high-Al basalts (Shervais et al. 1985; Gancarz et al. 1971; Longhi et al. 1972; Taylor et al. 1983).

Comparison of New Basalts to Previously Described Apollo 16 Basalts

Only 20 crystalline basalts from the Apollo 16 site have been previously described (see Table 7 for a summary with references). Of these, only five are greater than 1 mm in size and the largest is ~1 cm in diameter. On the basis of the classifications of the original investigators, these basalt fragments can be divided into three main groups: high-Ti basalts similar to Apollo 17 mare basalts, low-Ti basalts that are often described as similar to the Apollo 12 ilmenite basalts, and high-Al basalts like those found at Luna 16. These classifications are based in large part on mineral chemistry and mineral zoning trends (e.g., Delano 1975), as bulk chemical compositions were only obtained for a few of the previously reported Apollo 16 basalts. The lack of bulk chemistry compositions for most of the previously studied Apollo 16 basalts makes a detailed comparison to the basalts of this study difficult and in some cases inconclusive.

Of the five samples of this study, only the Apollo 17–like high-Ti basalt 60503,22-7 clearly falls into one of the previously recognized groups. Fragments 65703,9-13 and 62243,10-22 are the first VLT basalts from the Apollo 16 site to be reported. Three of the five previously identified low-Ti basalts at the Apollo 16 site (see Table 7) are much smaller (<200 μm) than the fragments described in this study, and may be unrepresentative fragments of VLT basalts similar to

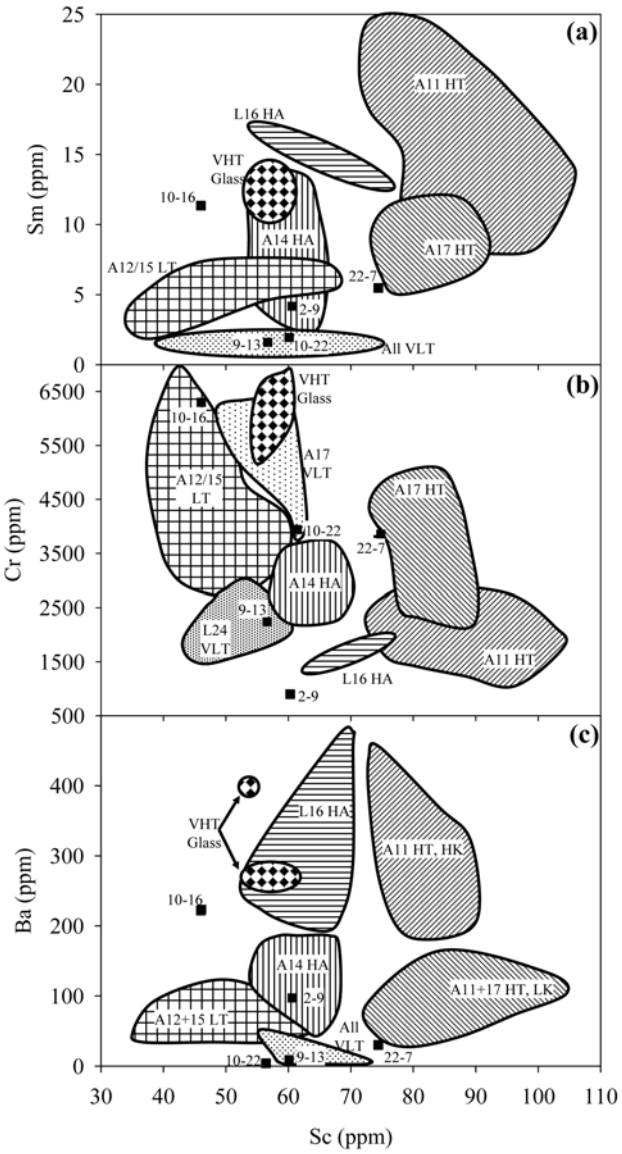

Fig. 6. Trace-element discrimination plots showing the fields for the known mare basalt suites with the samples from this study superimposed. a) Sc versus Sm: 60503,22-7 falls within the Apollo 17 high-Ti basalt field, 65703,9-13 and 62243,10-22 fall within the combined Luna 24 and Apollo 17 VLT field, 60603,10-16 has similar Sm concentrations, but lower Sc concentrations compared to the Apollos 12 and 14 very high-Ti glass field, and 60053,2-9 falls within the Apollo 14 high-Al basalt field. b) Sc versus Cr: 60503,22-7 falls within the Apollo 17 high-Ti basalt field, 65703,9-13 and 62243,10-22 fall within the Luna 24 and Apollo 17 VLT basalt fields respectively, 60603,10-16 has similar to Cr concentrations but lower Sc levels than the fields of the Apollos 12 and 14 very high-Ti pyroclastic samples, and 60053,2-9 has very low-Cr concentrations, far below any mare basalt field. c) Sc versus Ba: 60503,22-7 falls very near the Apollo 11 and 17 high-Ti basalt field (with slightly lower Ba), 65703,9-13 and 62243,10-22 fall in or very near the combined Apollo 17 and Luna 24 VLT field, 60603,10-16 has slightly lower Ba and Sc levels than the Apollo 12 and 14 red-black pyroclastic glass samples, and 60053,2-9 falls within the Apollo 14 high-Al basalt field.

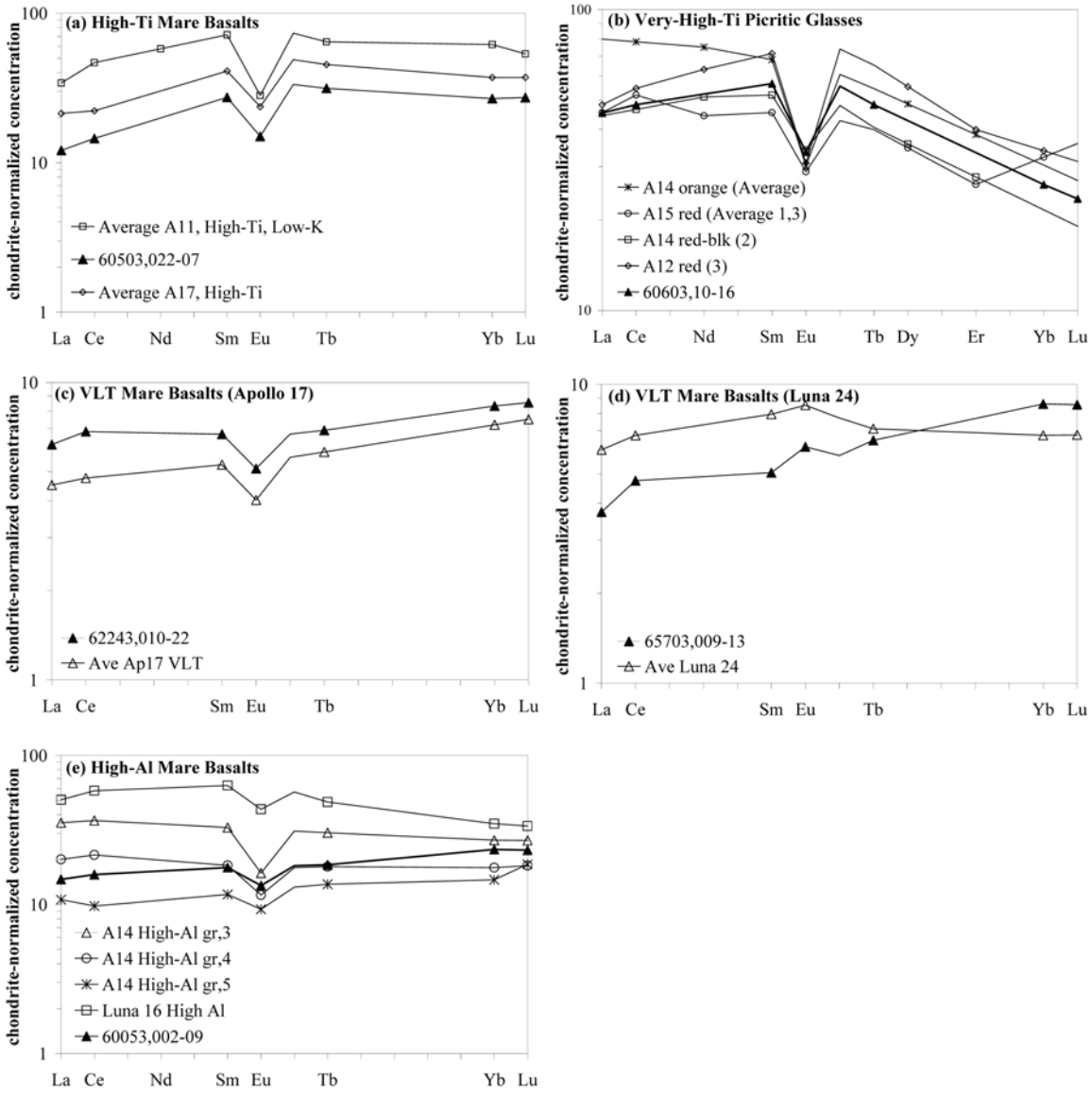

Fig. 7. Chondrite-normalized REE plots comparing the mare basalts in this study to known literature groups or samples. a) Proposed high-Ti mare basalt 60503,22-7 has a near-identical REE pattern and similar REE concentrations compared to average Apollo 17 high-Ti basalts. b) Proposed very high-Ti basaltic glass sample 60603,10-16 has an REE pattern and REE concentrations that are very similar to both Apollo 14 red-black glass and Apollo 12 red glass. c) Proposed VLT mare basalt 62243,10-22 has an REE pattern and REE concentrations that are very similar to average Apollo 17 VLT mare basalts. d) Proposed VLT mare basalt 65703,9-13 has a positive Eu anomaly, light REE pattern, and REE concentrations that are similar to average Luna 24 VLT mare basalts. The heavy REE pattern is not similar, however. e) Proposed high-Al mare basalt 60053, 2–9 has an REE-pattern very similar to average Apollo 14 high-Al group 5.

those found in this study. The very high-Ti pyroclastic glass 60603,10-16 is unlike any sample previously reported from the Apollo 16 site. A few high-Ti picritic glasses have been found in Apollo 16 soils (Delano 1975), but they were similar to the high-Ti orange glasses at the Apollo 17 site (~8 wt% TiO_2), and geochemically distinct from 60603,10-16.

The high-Al basalt reported in this study (60053,2-9) is similar to Apollo 14 high-Al basalts, particularly group 5. The Apollo 16 samples (60639,1 and 60019,Ba-2) previously classified as Luna 16–like high-Al basalts (Delano 1975; Takeda et al. 1987) might, in fact, both be high-Ti basalts. Fragment 60639,1 has ~7.5 wt% TiO_2 and was described by one set of investigators (Murali et al. 1976) as a high-Ti basalt similar to the Apollos 11 and 17 high-Ti mare basalts. Sample 60019,Ba-2 also has ~7.5 wt% TiO_2 (Takeda et al. 1987), but only has 17 wt% FeO + MgO, and may instead be an impact-melt rock. Sample 60053,2-9 may represent the first high-Al basalt of any kind found at the site and is almost certainly the first Apollo 14–like high-Al basalt identified at the Apollo 16 site.

DISCUSSION

Thus far in this paper, we have only discussed the relatively large (usually crystalline) basalt fragments found at the Apollo 16 site. However, the bulk of the basaltic component in mature Apollo 16 soils is not composed of this material. Two surveys of 2–4 mm particles from mature Apollo 16 soils (this work and Delano et al. 1973) found that basalts make up only ~1% by mass of the 2–4 mm size fraction of mature Cayley soils, and only a single basalt fragment >4 mm (66043,2,17) was found in the Apollo 16 soils. In contrast, mass-balance modeling of the composition of the Apollo 16 regolith (mature samples distant from North Ray Crater) requires that the <1 mm fines consist of 6.0% ± 1.4% basaltic material in order to account for the high concentrations of Sc, Cr, and Fe compared to the nonmare rocks of which the regolith is mainly composed (Korotev 1997). Petrographic studies of the <1 mm grain-size fraction have shown that the majority of the basaltic material in this grain size is present as green, yellow, and orange basaltic glass, with very few fragments of crystalline basalt observed (Heiken et al. 1973; Kempa and Papike 1980; Houck 1982a, 1982b; Basu and McKay 1984; Zeigler et al. 2004).

The basaltic glass at the Apollo 16 site has its own tale to tell, which we will present elsewhere (Zeigler et al., Forthcoming). It is necessary to mention the basaltic glass here because although the discussion that follows about the transport and provenance of basaltic materials was formulated with large lithic basalt fragments in mind, it also applies to the bulk of the Apollo 16 basaltic component, which comprises small basaltic glass fragments.

What is the Transport Mechanism for Basaltic Material at the Apollo 16 Site?

Any and all basaltic material that occurs in the Apollo 16 regolith must have originated from at least a couple hundred kilometers away, transported to the site as impact ejecta. The nearest mare is ~220 km to the east-northeast (Sinus Asperitatis) (Fig. 1); no cryptomare deposits (Schultz and Spudis 1979, 1983; Head and Wilson 1992) or pyroclastic deposits (Gaddis et al. 1985; Hawke et al. 1989) have been mapped in the area. Furthermore, the nearest pyroclastic deposits (500–600 km; Gaddis et al. 1985; Hawke et al. 1989) are considerably farther away than the maximum eruptive distances of lunar pyroclastics (<300 km; Head and Wilson 1979; Wilson and Head 1981). This leaves impact processes as the only transport mechanism operating on the Moon which could have deposited basaltic material at the Apollo 16 site.

With regard to basaltic material at the Apollo 16 site, the most significant question is whether the material was emplaced at the site during the time of basin formation early in the Moon's history or by post-basin impacts of crater-forming meteoroids. Ejecta from at least three major basins,

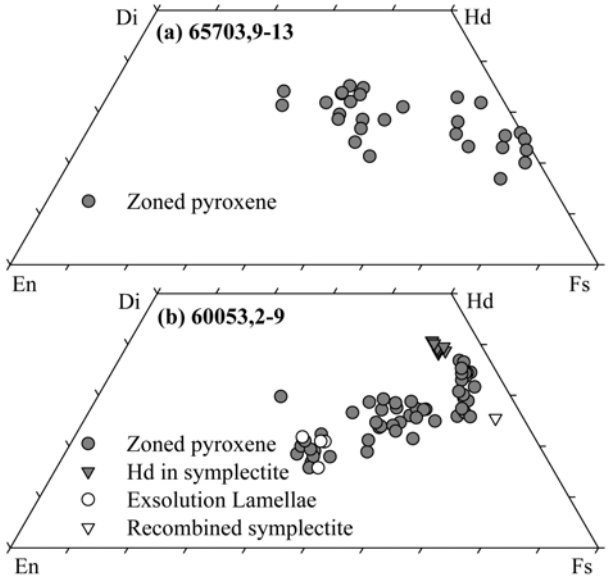

Fig. 8. a) Composition of the zoned pyroxene in crystalline basalt 65703,9-13. b) The composition of zoned pyroxene grains in the coarse-grained basalt 60053,2-9. Recombined symplectite composition is based on broad-beam EMPA.

Nectaris, Serenitatis, and Imbrium, were deposited at the Apollo 16 site (Spudis 1984; Stöffler et al. 1985; Wilhelms 1987) and in some models, less than half the material in the present regolith occurred in the vicinity of the site prior to the Nectaris impact (Haskin et al. 2002, 2003). Nevertheless, we think that the fragments of mare basalt in the Apollo 16 regolith are mainly from dispersal of material by smaller post-basin impacts into maria for three reasons.

First, one of the basaltic fragments previously recovered from an Apollo 16 soil, 66043,2,17 (Table 7), has been dated by Schaeffer and Husain (1974) at 3.79 ± 0.05 Ga by the Ar-Ar technique. This basalt fragment was classified as a high-Ti basalt similar to those found at the Apollo 17 site (Delano 1975), and it is compositionally similar to sample 60503,22-7 in this study and other high-Ti basalts at the Apollo 16 site (see Table 7). Although this is only one sample, it shows that at least some of the Apollo 16 basalt (particularly the high-Ti samples) was deposited at the site by post-basin impacts into the surrounding maria.

Second, numerous breccias at the Apollo 16 site, known collectively as the ancient regolith breccias (McKay et al. 1986), have the property that they are composed of regolith lithified at the time of basin formation, about 4 Ga ago. Since then, the ancient regolith breccias have been closed to addition of new material. The ancientness of the breccias is witnessed by high $^{40}Ar/^{36}Ar$ ratios and excess fission Xe compared with regolith occurring at the surface of the Moon today (McKay et al. 1986). These noble gas observations require that some of the material of which the ancient regolith breccias are composed existed as fine-grained material at the surface of the Moon early in lunar history. The ancient

Table 7. Summary of Apollo 16 crystalline mare basalts.

Sample number	Type of parent sample	Basalt classification	Particle size	Minerals: present/compositions				Major elem.	Trace elem.	References[a]
				Pyx	Olv	Plag	Oxide			
60639,1	Clast in frag. brec.[b]	Luna 16 high-Al[c]	1 cm	Yes/yes	Yes/yes	Yes/yes	Yes/yes	Yes	Yes	1–4
66043,2,17	Rake sample	Ap17 high-Ti	7 mm	Yes/yes	Yes/yes	Yes/yes	Yes/yes	No	No	1, 5
61501,630	Soil fragment	Ap17 high-Ti	450 um	Yes/yes	Yes/yes	Yes/no	Yes/yes	No	No	1
60003,230	Clast in drill core	High-Ti	200 um	Yes/yes	Yes/no	Yes/no	Yes/no	No	No	1
60003,246	Clast in drill core	Ap12 ilm	100 um	Yes/yes	Yes/yes	Yes/no	Yes/no	No	No	1
60003,248	Clast in drill core	High Al, low-Ti	150 um	Yes/yes	No/no	Yes/no	Yes/no	No	No	1
60003,250	Clast in drill core	Low Al, low-Ti	200 um	Yes/yes	No/no	Yes/no	Yes/no	No	No	1
60019,Ba-1	Clast in reg. brec.	Inconclusive[d]	2.5 mm	Yes/no	No/no	Yes/no	Yes/no	No	No	6
60019,Ba-2	Clast in reg. brec.	Luna 16 high-Al[d]	5 mm	Yes/yes	No/no	Yes/yes	Yes/yes	Yes	No	6, 7
60255,21	Clast in reg. brec.	Ap15 pigeonite	7 mm	Yes/yes	No/no	Yes/yes	Yes/yes	Yes	No	8
60009/10,A	Clast in drill core	Ap17 high-Ti	500 um	Yes/yes	Yes/yes	Yes/yes	Yes/no	No	No	9
60009/10,B	Clast in drill core	Ap12 ilm	> 1 mm	Yes/yes	no/no	Yes/yes	Yes/no	No	No	9
67915,	Clast in 67915	Inconclusive[d]	300 um	Yes/yes	Yes/yes	Yes/yes	Yes/no	No	No	10

[a]Listed classifications are those of the original authors: 1) Delano 1975; 2) Dowty et al. 1974a; 3) Dowty et al. 1974b; 4) Murali et al. 1976; 5) Schaffer and Husain 1974; 6) Takeda et al. 1987; 7) Galindo 1985; 8) Simon and Papike 1987; 9) Vaniman et al. 1978 (seven other lithic basalt fragments were found and mentioned but not described); 10) Roedder and Weiblen 1974.

[b]Reg. brec. = regolith breccia, frag. = fragmental.

[c]Classification of investigators 1–3. Was also classified as an Apollo 11 low-K, high-Ti basalt by 4).

[d]The classification of these particles as mare basalts is debatable; they could both be mafic impact-melt clasts. Sample 66043,2,17 had an Ar-Ar date reported).

regolith breccias of Apollo 16 contain clasts of mafic, Th-rich impact-melt breccias that are identical in composition to those impact-melt breccias that occur as large rocks and from which basin ages are usually determined (Korotev 1996). Together these observations suggest that the ancient regolith breccias were formed during or just after the Imbrium impact (Korotev 1997).

Although the ancient regolith breccias of Apollo 16 are similar in composition to the present Apollo 16 regolith and to young regolith breccias (Jerde et al. 1990) that do not have the distinctive noble gas signature of old regolith, they are compositionally distinct in being poorer in those elements that are most enriched in mare basalt, namely Sc and Cr. No mare-derived material was found in an INAA study of large clasts in the ancient regolith breccias (Korotev 1996) and petrographic studies of the submillimeter clasts in ancient regolith breccias (Wentworth and McKay 1988; Simon et al. 1988) found only three suspected mare glasses (FeO > 15 wt%, $CaO/Al_2O_3 > 0.75$) and a few suspected mare lithic fragments. We interpret the paucity of mare material in the ancient regolith breccias as strong evidence that there was little to no mare material present at the Apollo 16 site following the last major basin-forming event that influenced the site, i.e., Imbrium.

The third line of evidence that the basin ejecta deposits contained little mare material is that mare material is rarer in the ejecta deposit of North Ray Crater than it is elsewhere at the site. The North Ray Crater impact event occurred in geologically recent times, ~50 Ma (Arvidson et al. 1975). As a 1 km crater, North Ray Crater excavated material from depths up to about 200 m (the transient crater radius is about 70% of the observed crater radius, and the ratio of excavation depth to transient crater radius for simple craters is about 1:5) (Melosh 1989). This is significant because most of the material excavated by North Ray Crater would likely not contain any material added to the Apollo 16 site since the formation of the Apollo 16 site (post-Imbrium).

Studies both of rocks (Roedder and Weiblen 1974; Nord et al. 1975; James 1981; Stöffler et al. 1981, 1985; Lindstrom and Salpas 1983) and of small rock fragments (Jolliff and Haskin 1995) from the regolith ejected from North Ray Crater have yielded only a single possible basalt clast (300 μm) in breccia 67915 (Roedder and Weiblen 1974). The compositions of North Ray Crater soils show none of the chemical signatures of mare basalt that is shown by the soils more distant from the craters (Korotev 1996). Overall, the evidence suggests that there was little if any mare material present at the Apollo 16 site following the Imbrium impact event. Thus, the basaltic component of the Apollo 16 regolith must derive mainly from post-basin impacts into maria.

Provenances of Basaltic Materials at the Apollo 16 Site

We speculate on the sources of mare material in the Apollo 16 regolith first by making the assumption that any given fragment is more likely to have come from a nearby mare than a distant mare and then by comparing the composition of the fragment to compositions inferred for nearby mare from remote sensing techniques. Recent ejecta modeling (Haskin et al. 2002, 2003) predicts that a crater 300 km from the Apollo 16 site will deposit approximately four times more material at the Apollo 16 site than if the same crater was 600 km away, illustrating that with increasing distance, the likelihood that ejecta from a given impact into a maria is the source of the basaltic material at the Apollo 16 site falls off dramatically. If ejecta from a 3.6 km lunar crater can make it all the way to Earth (in the form of lunar meteorites) (Melosh 1985), however, any provenance assigned to basaltic material found at the Apollo 16 site cannot be absolutely proven. At extreme distances the modeling of ejecta deposits becomes a stochastic process that does not lend itself well to quantitative modeling.

We use Clementine UVVIS data at 1 km resolution to identify the most likely source regions for the basaltic materials sampled at the Apollo 16 site. This task is accomplished by comparing the Clementine-derived FeO and TiO_2 maps (Fig. 9), using the algorithms described in Gillis et al. (2003, 2004), with the concentrations of those elements measured in the Apollo 16 basalt samples. We acknowledge that the element distribution maps in Fig. 9 represent the composition of mare surfaces, that is, regoliths developed on mare basalt that have had varying amounts of highlands material added, not the original mare basalt flows themselves. The lower TiO_2 concentrations in mare soils due to dilution by highlands material are not really an issue here, however, as the differences in the TiO_2 concentrations among the main compositional groups of Apollo 16 basaltic material (e.g., VLT/low-Ti versus high-Ti) and of the maria closest to the Apollo 16 site (Sinus Asperitatis, Mare Nectaris, Mare Tranquillitatis) are considerably greater than the variation due to highlands contamination.

High-Ti Basaltic Material

The high-Ti mare basalt flows nearest to the Apollo 16 site are in southern Mare Tranquillitatis (~7–10 wt% TiO_2), about 300 km northeast from the Apollo 16 site. The next nearest high-Ti mare basalt flows are approximately 600 km north in portions of Mare Vaporum and ~750 km west in portions of eastern Mare Nubium. In addition to being more distant, these last two sites are smaller than Mare Tranquillitatis and have TiO_2 concentrations (6–7 wt% TiO_2) that are only marginally high-Ti. Because it is by far the closest and the most extensive, Mare Tranquillitatis is the most likely source region for the Apollo 16 high-Ti mare basalts. Several small Eratosthenian and Copernican craters lie in the southwestern portion of Mare Tranquillitatis and are candidate source craters: Dionysius, Ross, Arago, Maskelyne, Moltke, Sosigenes, and Schmidt (Fig. 9) (Morris and Wilhelms 1967; Milton 1968). Dionysius is particularly

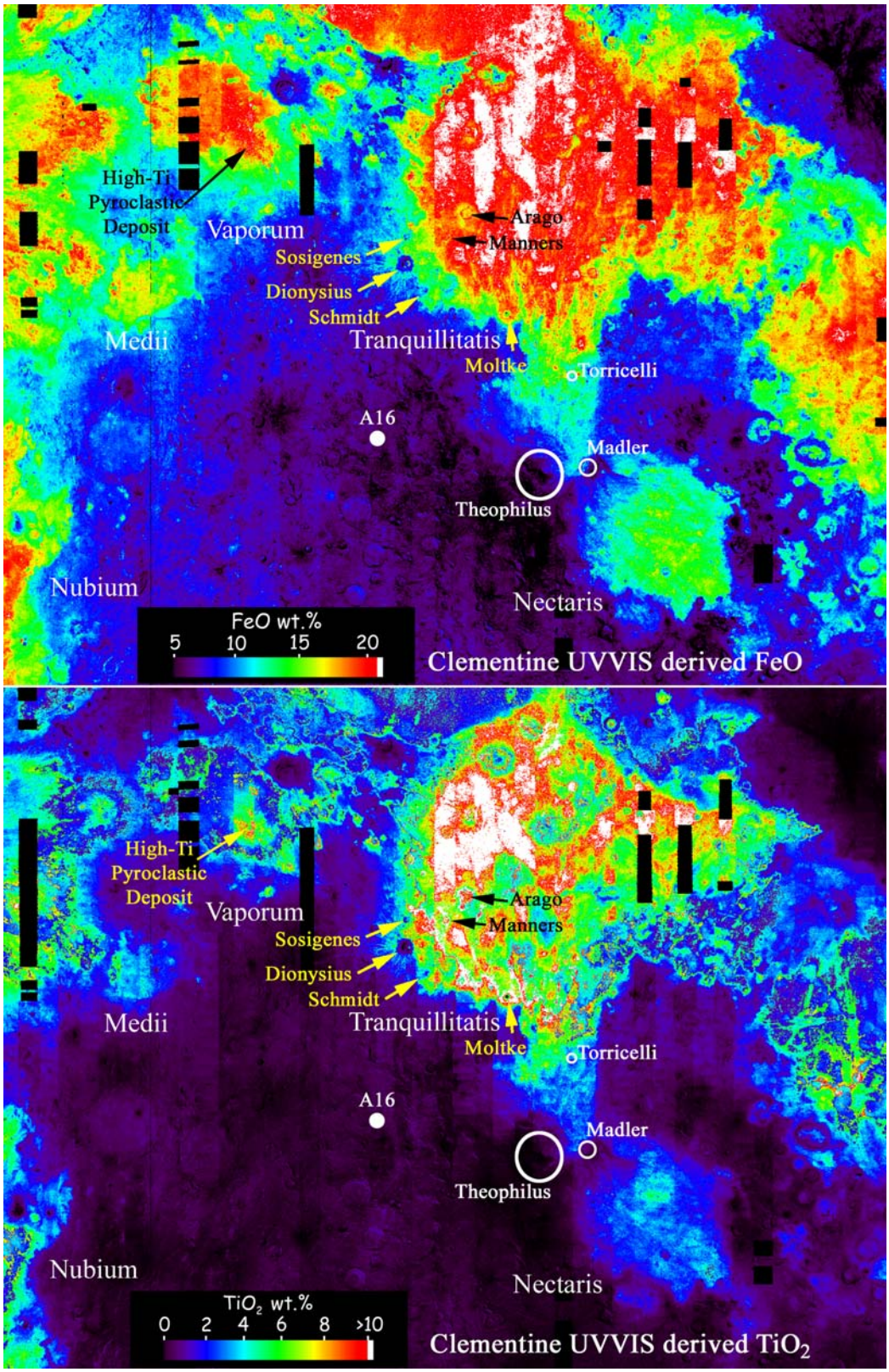

Fig. 9. Clementine UVVIS derived FeO (top) and TiO_2 (bottom) maps (at 1 km resolution) based on the equations of Gillis et al. (2003, 2004) showing the Apollo 16 site and the major maria around it. Probable source craters in Mare Nectaris for low-Ti basaltic material at the Apollo 16 site are shown in white (with crater rim outlined) and probable source craters in Mare Tranquillitatis for high-Ti basaltic material at the Apollo 16 site are indicated by black and yellow arrows.

attractive as a source crater because it has rays that are elevated in both TiO_2 and FeO that extend into the highlands directly toward the Apollo 16 site (Fig. 9).

Low-Ti Basaltic Material

The low-Ti mare basalt flows nearest to the Apollo 16 site are in Sinus Asperitatis and Mare Nectaris. The current edges of these maria are about 220 km and 400 km distant respectively (Wilhelms and McCauley 1971). The edge of Mare Nectaris was much closer to the Apollo 16 site (likely ~250 km) before the impact of Theophilus, a 100 km Copernican age crater on the western edge of Mare Nectaris. Pieters (1978) has mapped Mare Nectaris and Sinus Asperitatis as compositionally uniform on the basis of Earth-based remote sensing. Hereafter, we will refer to the basalt flows in the Mare Nectaris-Sinus Asperitatis region collectively as Mare Nectaris. The next closest low-Ti maria are Sinus Medii (~500 km northwest) and Mare Vaporum (~600 km north-northwest), both of which are much less extensive than Mare Nectaris.

On the basis of areal extent and proximity, Mare Nectaris is the most likely source region for low-Ti basaltic material at the Apollo 16 site. Given the size of Theophilus, its proximity to the Apollo 16 site, and the presence of secondary craters within 10 km of the Apollo 16 site that are mapped as Theophilus secondary craters (Milton and Hodges 1972), it is almost certain that Theophilus delivered basaltic material to the Apollo 16 site. Two other Copernicanage craters, Madler and Torricelli (both ~30 km), occur in Mare Nectaris and could also have deposited low-Ti basaltic material at the Apollo 16 site.

VLT Mare Basaltic Material

The detection limit for TiO_2 concentrations derived from remotely sensed Clementine UVVIS data is about 1 wt%, making it difficult to distinguish VLT basalts (<1 wt% TiO_2) from some low-Ti basalts (1–5 wt% TiO_2). Furthermore, impact mixing with higher TiO_2 mare units can mask the presence of VLT basalt flows. Mare Frigoris contains the only large expanse of mare basalt that has been mapped as VLT. Mare Frigoris is nearly 1500 km from the Apollo 16 site, however, making it an unlikely source region. Some Clementine pixels in nearby Mare Nectaris have TiO_2 concentrations as low as 0.9 wt%, and Mare Nectaris has an average concentration of ~2.5 wt%. The range of TiO_2 concentrations in Mare Nectaris exceeds that of VLT basalt, but it is comparable to large regions of Mare Crisium and Mare Serenitatis, which are the presumed sources of the VLT basalts currently in the sample set (Luna 24 and Apollo 17, respectively). On the basis of proximity and Clementine-derived TiO_2 concentrations, Mare Nectaris is the only likely source region for the VLT basalts found at the Apollo 16 site (62243,10-22 and 65703,9-13), with Theophilus, Madler, and Torricelli again as likely source craters.

Aluminous Basaltic Material

Although global Al_2O_3 data based on the Lunar Prospector neutron spectrometer are available, the low sensitivity and large pixel size (~150 km) are not sufficient to identify high-Al basalt flows (Prettyman et al. 2002). Therefore, the only way to ascertain the likely provenance of the high-Al basaltic material at the Apollo 16 site is using their TiO_2 concentrations. As discussed earlier, the two previously reported high-Al basalts from the Apollo 16 site (60639,1 and 60019,Ba-2) both have TiO_2 concentrations >7 wt%, so regardless of whether or not they are truly high-Al basalts, Mare Tranquillitatis is their most likely source region. The high-Al basalt from this study (60053,2-9) is chemically similar to Apollo 14 group 5 high-Al basalts, which are thought to be Imbrium basin ejecta deposits (Dickinson et al. 1985; Shervais et al. 1985). Because the Cayley Plains of the Apollo 16 site are an ejecta deposit from the Imbrium impact (Wilhelms 1987; Stöffler 1981, 1985; Spudis 1984), it is possible that the source region for high-Al mare basalt fragment 60053,2-9 is also as Imbrium ejecta. Because fragment 60053,2-9 has little to no discernible KREEP component, an origin within the Procellarum KREEP Terrane is not indicated, however. With a TiO_2 concentration of ~2 wt%, fragment 60053,2-9 could also have an origin in Mare Nectaris, with Theophilus again as a likely source crater.

Pyroclastic Material

Although rare, VLT (Delano 1986; Shearer and Papike 1993), high-Ti (Delano 1975), and very high-Ti pyroclastic glasses (this work) have been identified in the Apollo 16 regolith. Very low-Ti pyroclastic glass particles have been identified in the regolith of every Apollo site, but as yet not a single definitive VLT pyroclastic deposit has been identified (Gaddis et al. 1985). Therefore, we are not able to speculate on the possible origin of Apollo 16 VLT pyroclastic material with any degree of certainty.

As stated earlier, the nearest high-Ti or very high-Ti pyroclastic deposits to the Apollo 16 site are the large regional deposit just south of Mare Vaporum (~25,000 km^2) (Wilhelms 1968), and smaller local pyroclastic deposits about 500 km away in Alphonsus crater and along the northern and southern edge of Mare Nectaris (<200 km^2) (Wilhelms and McCauley 1971). The algorithm for deriving TiO_2 concentrations from Clementine UVVIS spectra is not appropriate for glassy samples, so precise concentrations cannot be obtained. The UVVIS spectra of these areas, along with their low albedo, indicate that all of them are high in TiO_2. As the Vaporum deposit is two orders of magnitude

larger in area than the Nectaris deposits and are only marginally farther away, it seems to be the more likely source for high-Ti and very high-Ti basaltic material at the Apollo 16 site. No likely source crater is evident, however.

CONCLUSIONS

Five new basaltic fragments were found among 506 2–4 mm particles from the Apollo 16 soils, doubling the number of >1 mm mare basalts recovered from the Apollo 16 site. These new mare volcanic fragments include a high-Ti mare basalt, two VLT mare basalts, an aluminous mare basalt, and a very high-Ti pyroclastic glass fragment. The high-Ti basalt is similar to basalts from the Apollo 16 site observed previously, but all of the other basalts analyzed are of types not previously reported for the Apollo 16 site. These basaltic samples augment compositional and mineralogical information on the lunar mare basalt suite and they yield information about the composition of the maria surrounding the Apollo 16 site, some of which (e.g., Mare Nectaris) were not directly sampled.

The mare basalts from the Apollo 16 site are post-Imbrium additions to the regolith, based on the absence of mare basalt in the Apollo 16 ancient regolith breccias or in ejecta from North Ray Crater. The likely sources of the mare basalts are small- to medium-sized craters in the surrounding maria, particularly Theophilus, Madler, and Torricelli in Mare Nectaris (VLT, high-Al, and low-Ti basalts) and Ross, Arago, Dionysius, Maskelyne, Moltke, Sosigenes, and Schmidt in southern Mare Tranquillitatis (high-Ti basalts).

Acknowledgments–We thank Ms. Kaylynn Rockow for assistance with INAA preparation and Dr. Daniel Kremser for help with the electron microprobe. Informal reviews of the manuscript by Dr. Robert F. Dymek, Dr. Andrew Dombard, and Dr. Robert Tucker improved the manuscript and were much appreciated. Thorough reviews by Dr. John Delano, Dr. Steve Simon, and Dr. Kevin Righter were much appreciated and greatly improved the quality of the finished manuscript. This work was supported through NASA grant NAG5-10485 (L. Haskin).

Editorial Handling—Dr. Kevin Righter

REFERENCES

Arvidson R., Crozaz G., Drozd R. J., Hohenberg C. M., and Morgan C. J. 1975a. Cosmic ray exposure ages of features and events at the Apollo landing sites. *The Moon* 13:259–276.

Basu A. and McKay D. S. 1984. Petrologic comparisons of Cayley and Descartes on the basis of Apollo 16 soils from stations 4 and 11. Proceedings, 15th Lunar and Planetary Science Conference. pp. B535–B541.

Blanchard D. P., Brannon J. C., Aaboe E., and Budahn J. R. 1978. Major and trace element chemistry of Luna 24 samples from Mare Crisium. In *Mare Crisium: The view from Luna 24*, edited by Merrill R. B. and Papike J. J. New York: Pergamon Press. pp. 613–630.

Delano J. W. 1975. Petrology of the Apollo 16 mare component: Mare Nectaris. Proceedings, 6th Lunar Science Conference. pp. 15–47.

Delano J. W. 1986. Pristine lunar glasses: Criteria, data, and implications. Proceedings, 16th Lunar and Planetary Science Conference. pp. D201–D213.

Delano J. W., Bence A. E., Papike J. J., and Cameron K. L. 1973. Petrology of the 2–4 mm soil fraction of the Moon and stratigraphic implications. Proceedings, 4th Lunar Science Conference. pp. 537–551.

Dickinson T., Taylor G. J., Keil K., Schmitt R. A., Hughes S. S., and Smith M. R. 1985. Apollo 14 aluminous mare basalts and their possible relationship to KREEP. Proceedings, 15th Lunar and Planetary Science Conference. pp. C365–374.

Dowty E., Keil K., and Prinz M. 1974a. Igneous rocks from Apollo 16 rake sample (abstract). Proceedings, 5th Lunar Science Conference. pp. 174–176.

Dowty E., Keil K., and Prinz M. 1974b. Igneous rocks from Apollo 16 rake samples. Proceedings, 5th Lunar Science Conference. pp. 431–445.

Gaddis L. R., Pieters C. M., and Hawke B. R. 1985. Remote sensing of lunar pyroclastic mantling deposits. *Icarus* 61:461–489.

Galindo C. 1985. Regolith breccia 60019. *Lunar Sample Newsletter* 43:23–37.

Gancarz A. J., Albee A. L., and Chodos A. A. 1971. Petrologic and mineralogic investigation of some crystalline rocks returned by the Apollo 14 mission. *Earth and Planetary Science Letters* 12: 1–18.

Gillis J. J., Jolliff B. J., and Korotev R. L. 2004. Lunar surface geochemistry: Global concentrations of Th, K, and FeO as derived from Lunar Prospector and Clementine data. *Geochimica et Cosmochimica Acta* 68:3791–3805.

Gillis J. J., Jolliff B. L., and Elphic R. C. 2003. A revised algorithm for calculating TiO_2 from Clementine UVVIS data: A synthesis of rock, soil, and remotely sensed TiO_2 concentrations. *Journal of Geophysical Research*, doi:10.1029/2001JE001515.

Haskin L. A., Korotev R. L., Gillis J. J., and Jolliff B. L. 2002. Stratigraphies of Apollo and Luna highland landing sites and provenances of materials from the perspective of basin impact ejecta modeling. (abstract #1364) 33rd Lunar and Planetary Science Conference. CD-ROM.

Haskin L. A., Moss B. E., and McKinnon W. 2003. On estimating ejecta deposit thicknesses and proportions of materials from distant basins at lunar highland sites. *Meteoritics & Planetary Science* 38:13–34.

Hawke B. R., Coombs C. R., Gaddis L. R., Lucey P. G., and Owensby P. D. 1989. Remote sensing and geologic studies of localized dark mantle deposits on the Moon. Proceedings, 19th Lunar and Planetary Science Conference. pp. 255–268.

Head J. W. and Wilson L. 1979. Aphonsus-type dark halo craters: Morphology, morphometry and eruption conditions. Proceedings, 10th Lunar and Planetary Science Conference. pp. 2861–2897.

Head J. W. and Wilson L. 1992. Lunar mare volcanism: Stratigraphy, eruption conditions, and the evolution of secondary crusts. *Geochimica et Cosmochimica Acta* 56:2155–2175.

Heiken G. H., McKay D. S., and Fruland R. M. 1973. Apollo 16 soils: Grain size analyses and petrography. Proceedings, 4th Lunar Science Conference. pp. 251–265.

Houck K. J. 1982a. Modal petrology of six soils from Apollo 16 double drive tube core 64002. Proceedings, 13th Lunar and Planetary Science Conference. pp. A210–A220.

Houck K. J. 1982b. Petrologic variations in Apollo 16 surface soils.

Proceedings, 13th Lunar and Planetary Science Conference. pp. A197–A209.
James O. B. 1981. Petrologic and age relations of the Apollo 16 rocks: Implications for subsurface geology and the age of the Nectaris Basin. Proceedings, 12th Lunar and Planetary Science Conference. pp. 209–233.
Jolliff B. L. and Haskin L. A. 1995. Cogentic rock fragments from a lunar soil: Evidence of a ferroan noritic-anorthosite pluton on the Moon. *Geochimica et Cosmochimica Acta* 59:2345–2374.
Jolliff B. L., Korotev R. L., and Haskin L. A. 1991. Geochemistry of 2–4 mm particles from Apollo 14 soil (14161) and implications regarding igneous components and soil-forming processes. Proceedings, 21st Lunar and Planetary Science Conference. 21: 193–219.
Jolliff B. L., Rockow K. M., Korotev R. L., and Haskin L. A. 1996. Lithologic distribution and geologic history of the Apollo 17 site: The record in soils and small rock particles from the highland massifs. *Meteoritics & Planetary Science* 31:116–145.
Jolliff B. L., Rockow K. M., and Korotev R. L. 1998. Geochemistry and petrology of lunar meteorite Queen Alexandra Range 94281, a mixed mare and highland regolith breccia, with special emphasis on very-low-Ti mafic components. *Meteoritics & Planetary Science* 33:581–601.
Kempa M. J. and Papike J. J. 1980. The Apollo 16 regolith: Comparative petrology of the >20 μm and 10–20 μm soil fractions, lateral transport and differential volatilization. Proceedings, 11th Lunar and Planetary Science Conference. 11: 1635–1661.
Korotev R. L. 1991. Geochemical stratigraphy of two regolith cores from the central highlands of the Moon. Proceedings, 21st Lunar and Planetary Science Conference. pp. 229–289.
Korotev R. L. 1994. Compositional variation in Apollo 16 impact-melt breccias and inferences for the geology and bombardment history of the Central Highlands of the Moon. *Geochimica et Cosmochimica Acta* 58:3931–3969.
Korotev R. L. 1996. On the relationship between the Apollo 16 ancient regolith breccias and feldspathic fragmental breccias, and the composition of the prebasin crust in the Central highlands of the Moon. *Meteoritics & Planetary Science*. 31:403–412.
Korotev R. L. 1997. Some things we can infer about the Moon from the composition of the Apollo 16 regolith. *Meteoritics & Planetary Science* 32:447–478.
Korotev R. L., Jolliff B. L., Zeigler R. A., and Haskin L. A. 2003. Compositional constraints on the launch pairing of three brecciated lunar meteorites of basaltic composition. *Antarctic Meteorite Research* 16:152–175.
Lindstrom D. J. and Korotev R. L. 1982. TEABAGS: Computer programs for instrumental neutron activation analysis. *Journal of Radioanalytical and Nuclear Chemistry* 70:439–458.
Lindstrom M. M. and Salpas P. A. 1983. Geochemical studies of feldspathic fragmental breccias and the nature of North Ray Crater ejecta. Proceedings, 13th Lunar and Planetary Science Conference. pp. A671–A683.
Longhi J. 1977. Magma oceanography 2: Chemical evolution and crustal formation. Proceedings, 8th Lunar Science Conference. pp. 602–621.
Longhi J., Walker D., and Hays J. F. 1972. Petrography and crystallization history of basalts 14310 and 14072. Proceedings, 3rd Lunar Science Conference. pp. 131–139.
Longhi J., Walker D., and Hays J. F. 1978. The distribution of Fe and Mg between olivine and lunar basaltic liquids. *Geochimica et Cosmochimica Acta* 42:1545–1558.
Ma M.-S., Schmitt R. A., Taylor G. J., Warner R. D., Lange D. E., and Keil K. 1978. Chemistry and petrology of Luna 24 lithic fragments and <250 μm soils: Constraints on the origin of VLT mare basalts. In *Mare Crisium: The view from Luna 24*, edited by Merrill R. B. and Papike J. J. New York: Pergamon Press. pp. 569–592.
Marvin U. B. and Walker D. 1978. Implications of titanium-rich glass clod at Oceanus Procellarum. *American Mineralogist* 63:924–929.
McKay D. S., Bogard D. D., Morris R. V., Korotev R. L., Johnson P., and Wentworth S. J. 1986. Apollo 16 regolith breccias: Characterization and evidence for early formation in the megaregolith. Proceedings, 16th Lunar and Planetary Science Conference. pp. D277–D303.
Melosh H. J. 1985. Ejection of rock fragments from planetary bodies. *Geology.* 13:144–148.
Melosh H. J. 1989. Impact cratering: A geologic process. *Oxford monographs on geology and geophysics*, no. 11. New York: Oxford University Press. 245 p.
Milton D. J. 1968. Geologic map of the Theophilus quadrangle of the Moon. Washington, D.C.: U.S. Geological Survey, Map I-546 (LAC-78).
Milton D. J. and Hodges C. A. 1972. Geologic map of the Descartes region of the Moon. Washington, D.C.: U.S. Geological Survey, Map I-748.
Morris E. C. and Wilhelms D. E. 1967. Geologic map of the Julius Caesar quadrangle of the Moon. Washington, D.C.: U.S. Geological Survey, Map I-510 (LAC-60).
Morris R. V. 1978. The surface exposure (maturity) of lunar soils: Some concepts and Is/FeO compilation. Proceedings, 9th Lunar and Planetary Science Conference. pp. 2287–2297.
Murali A. V., Ma M. -S., and Schmitt R. A. 1976. Mare basalt 60639, another eastern basin lunar basalt (abstract). Proceedings, 7th Lunar Science Conference. pp. 583–584.
Nord G. L., Christie J. M., Heuer A. H., and Lally J. S. 1975. North Ray Crater breccias: An electron petrographic study. Proceedings, 6th Lunar Science Conference. pp. 779–797.
Papike J. J. and Vaniman D. T. 1978. Luna 24 ferrobasalts and the mare basalt suite: Comparitive chemistry, mineralogy, and petrology. Proceedings, Mare Crisium: The view from Luna 24. pp. 371–401.
Papike J. J., Ryder G., and Shearer C. K. 1998. Lunar samples. In *Planetary materials*, edited by Papike J. J. Washington, D. C.: The Mineralogical Society of America. pp. 1–234.
Pieters C. M. 1978. Mare basalt types on the front side of the Moon: A summary of spectral reflectance data. Proceedings, 9th Lunar and Planetary Science Conference. pp. 2825–2849.
Prettyman T. H., Lawrence D. J., Vaniman D. T., Elphic R. C., and Feldman W. C. 2002. Classification of regolith materials from lunar prospector data reveals a magnesium-rich highland province (abstract). In *Moon beyond 2002: Next steps in lunar science and exploration*. Houston: Lunar and Planetary Institute. p. 22.
Roedder E. and Weiblen P. W. 1974. Petrology of clasts in lunar breccia 67915. Proceedings, 5th Lunar Science Conference. pp. 303–331.
Schaeffer O. A. and Husain L. 1974. Early lunar history: Ages of 2–4 mm soil fragments from the lunar highlands. Proceedings, 4th Lunar Science Conference. pp. 1847–1863.
Schultz P. H. and Spudis P. D. 1979. Evidence for ancient mare volcanism. Proceedings, 10th Lunar and Planetary Sciences Conference. pp. 2899–2918.
Schultz P. H. and Spudis P. D. 1983. Beginning and end of lunar mare volcanism. *Nature* 302:233–236.
Shearer C. K. and Papike J. J. 1993. Basaltic magmatism on the Moon: A perspective from volcanic picritic glass beads. *Geochimica et Cosmochimica Acta* 57:4785–4812.
Shervais J. W., Taylor L. A., and Lindstrom M. M. 1985. Apollo 14

mare basalts: Petrology and geochemistry of clasts from consortium breccia 14321. Proceedings, 15th Lunar and Planetary Science Conference. pp. C375–C395.

Simon S. B. and Papike J. J. 1987. Petrology of a low-titanium mare basalt from Apollo 16 regolith breccia 60255 (abstract). Proceedings, 18th Lunar and Planetary Science Conference. pp. 922–923.

Simon S. B., Papike J. J., Laul J. C., Hughes S. S., and Schmitt R. A. 1988. Apollo 16 regolith breccias and soils: Recorders of exotic component addition to the Descartes region of the Moon. *Earth and Planetary Science Letters* 89:147–162.

Spudis P. D. 1984. Apollo 16 site geology and impact melts: Implications for the geologic history of the lunar highlands. Proceedings, 15th Lunar and Planetary Science Conference. pp. C95–C107.

Stöffler D., Ostertag R., Reimold W. U., Borchardt R., Malley J., and Rehfeldt A. 1981. Distribution and provenance of lunar highland rock types at North Ray Crater, Apollo 16. Proceedings, 12th Lunar and Planetary Science Conference. pp. 185–207.

Stöffler D., Bischoff A., Borchardt R., Burghele A., Deutsch A., Jessberger E. K., Ostertag R., Palme H., Spettel B., Reimold W. U., Wacker K., and Wänke H. 1985. Proceedings, 15th Lunar and Planetary Science Conference. pp. C449–C506.

Takeda H., Miyamoto M., Galindo C., and Ishii T. 1987. Mineralogy of a basaltic clast in lunar highland regolith breccia 60019. Proceedings, 17th Lunar and Planetary Science Conference. pp. E462–E470.

Taylor L. A., Shervais J. W., Hunter R. H., Shih C.-Y., Bansal B. M., Wooden J., Nyquist L. E., and Laul L. C. 1983. Pre-4.2 AE mare-basalt volcanism in the lunar highlands. *Geochimica et Cosmochimica Acta* 66:33–47.

Vaniman D. T., Papike J. J., and Schweitzer E. L. 1978. The Apollo 16 double drive tube 60009/60010. Part II: Petrology and major element partitioning among the regolith components. Proceedings, 9th Lunar and Planetary Science Conference. pp. 1827–1860.

Wentworth S. J. and McKay D. S. 1988. Glasses in ancient and young Apollo 16 regolith breccias: Populations and Ultra Mg glass. Proceedings, 18th Lunar and Planetary Science Conference. pp. 67–77.

Wentworth S., Taylor G. J., Warner R. D., Keil K., Ma M.-S., and Schmitt R. A. 1979. The unique nature of Apollo 17 VLT basalts. Proceedings, 10th Lunar and Planetary Science Conference. pp. 207–223.

Wilhelms D. E. 1968. Geologic map of the Mare Vaporum Quadrangle of the Moon. Washington, D.C.: U.S. Geological Survey, Map I-548.

Wilhelms D. E. 1987. The geologic history of the Moon. U.S. Geological Survey Professional Paper #1348. Washington, D.C.: U.S. Geological Survey. 302 pp.

Wilhelms D. E. and McCauley J. F. 1971. Geologic map of the near side of the Moon. Washington, D.C.: U.S. Geological Survey, Map I-703.

Wilson L. and Head J. W. 1981. Ascent and eruption of basaltic magma on the Earth and Moon. *Journal of Geophysical Research* 86:2971–3001.

Zeigler R. A., Jolliff B. L., Korotev R. L., and Haskin L. A. 2000. Petrology, geochemistry, and possible origin of monomict mafic lithologies of the Cayley Plains (abstract #1859). 31st Lunar and Planetary Science Conference. CD-ROM.

Zeigler R. A., Korotev R. L., Jolliff B. L., Haskin L. A., and Floss C. 2004. Apollo 16 mafic glass: Geochemistry, provenance, and implications (abstract #2082) 35th Lunar and Planetary Science Conference. CD-ROM.

Zeigler R. A., Korotev R. L., Haskin L. A., Jolliff B. L., and Floss C. Forthcoming. The geochemistry and provenance of Apollo 16 mafic glasses. *Geochimica et Cosmochimica Acta* (Haskin special issue).